The Journal of Experimental Biology 201, 1563–1583 (1998)
Printed in Great Britain © The Company of Biologists Limited 1998
JEB1490

KINEMATIC MODELS OF THE BUCCAL MASS OF *APLYSIA CALIFORNICA*

RICHARD F. DRUSHEL[1], DAVID M. NEUSTADTER[2,*], ITAY HURWITZ[4,†], PATRICK E. CRAGO[2] AND HILLEL J. CHIEL[1,3,‡]

Departments of [1]Biology, [2]Biomedical Engineering and [3]Neurosciences, Case Western Reserve University, Cleveland, OH 44106-7080, USA and *[4]Department of Life Sciences, Bar-Ilan University, Ramat Gan 52900, Israel*

*Present address: MRI Division, Elscint Ltd, Advanced Technology Center, PO Box 550, Haifa 31004, Israel

†Present address: Department of Physiology and Biophysics, Box 1218, Mount Sinai School of Medicine, One Gustave Levy Place, New York, NY 10029, USA

‡Author for correspondence at address 1 (e-mail: hjc@po.cwru.edu)

Accepted 23 February; published on WWW 27 April 1998

Summary

The feeding behavior of the marine mollusc *Aplysia californica* is an intensively studied model system for understanding the neural control of behavior. Feeding movements are generated by contractions of the muscles of the buccal mass. These muscles are internal and cannot be visualized during behavior. In order to infer the movements of the muscles of the buccal mass, two kinematic models were constructed. The first kinematic model assumed that the complex consisting of the pincer-like radula and the underlying odontophore was spherical in shape. In this model, the radula/odontophore was moved anteriorly or posteriorly and the more superficial buccal muscles (I1/I3 and I2) were fitted around it. Although the overall buccal mass shapes predicted by this model were similar to those observed *in vivo* during protraction, the shapes predicted during retraction were very different. We therefore constructed a second kinematic model in which the shape of the radula/odontophore was based on the shapes assumed by those structures *in vitro* when they were passively forced into protraction, rest or retraction positions. As each of these shapes was rotated, the second kinematic model generated overall shapes of the buccal mass that were similar to those observed *in vivo* during swallowing and tearing, and made predictions about the antero-posterior length of the buccal mass and the relative location of the lateral groove. These predictions were consistent with observations made *in vivo* and *in vitro*. The kinematic patterns of intrinsic buccal muscles I1 and I2 *in vivo* were estimated using the second model. Both models make testable predictions with regard to the functions and neural control of intrinsic buccal muscles I2 and I3.

Key words: feeding, behaviour, muscular hydrostat, biomechanics, computational neuroethology, kinematic modelling, *Aplysia californica.*

Introduction

A first step towards understanding the mechanical properties of an animal's body is to study the movements that it makes during a behavior of interest and the way in which these movements are constrained by the geometry of the structure, i.e. by its kinematics. Second, one needs to understand how the musculature generates the forces that lead to these movements, i.e. its kinetics (Ozkaya and Nordin, 1991). For example, analysis of the kinematics and kinetics of human limb movements has been crucial for understanding neural control (Zajac, 1993) and for devising protocols for functional electrical stimulation (Yamaguchi and Zajac, 1990).

In order to combine studies of kinematics and kinetics with those of neural control, it is essential to have experimental preparations in which it is possible to study simultaneously both neural control and biomechanics. Invertebrates can be especially tractable to these studies, because they have identifiable neurons whose activity can be monitored as the biomechanics of the periphery during natural behaviors are studied. For example, Watson and Ritzmann (1997*a*,*b*) have recently characterized the leg kinematics and inferred the neural activity of identified leg motor neurons in the cockroach *Blaberus discoidalis* during slow and fast running.

Many studies of the neural basis of behavior have employed molluscan species, such as *Helisoma trivolvis* (Kater, 1974), *Aplysia californica* (Kandel, 1976), *Lymnaea stagnalis* (Elliott and Benjamin, 1985*a*,*b*), and *Tritonia diomedea* (Getting and Dekin, 1985), or other soft-bodied animals such as leeches (Lockery and Kristan, 1990*a*,*b*; Wittenberg and Kristan, 1992*a*,*b*), but until recently there have been relatively few studies of the biomechanics of these animals (Chapman, 1958, 1975; DeMont, 1992). Over a decade ago, a particular subclass of structures with hydrostatic skeletons was identified in which there is no central fluid cavity, so that the entire structure is made of muscle. These structures, termed

muscular hydrostats (Kier and Smith, 1985), are exemplified by tongues, trunks or tentacles. Because there are no hard skeletal elements to constrain movement to joints, these structures have fewer constraints on their degrees of freedom. How do the properties of these structures constrain or simplify neural control?

Several recent studies have addressed both the neural control and the biomechanics of hydrostatic skeletons and muscular hydrostats. A model of the body of the leech has been described (Skierczynski *et al.* 1996) in which many aspects of its geometry are realistically described and the parameters describing the passive and active properties of its body wall muscles are based upon experimental data (Wilson *et al.* 1996*b*). This model has been used successfully to examine the movements generated by crawling motor programs and has provided evidence that crawling motor patterns observed *in vitro*, in the absence of sensory feedback, do not generate normal movements or internal pressures, unlike motor patterns recorded *in vivo* (Wilson *et al.* 1996*a*; Kristan *et al.* 1998). Hydrostatic models of tongues and tentacles have recently been published (Chiel *et al.* 1992; van Leeuwen and Kier, 1997; van Leeuwen, 1997).

In order to study neural control and biomechanics simultaneously, we have focused on the feeding apparatus (the buccal mass) of the marine mollusc *Aplysia californica*. Over the last two decades, there have been extensive studies of the neural basis of many aspects of the feeding behavior of *Aplysia* species, including neural mechanisms of arousal (Weiss *et al.* 1978, 1981; Kupfermann and Weiss, 1982; Rosen *et al.* 1989), behavioral choice (Teyke *et al.* 1990), extrinsic and intrinsic modulation (Weiss *et al.* 1992; Katz and Frost, 1996), the motor pattern generators involved in feeding (Plummer and Kirk, 1990; Hurwitz *et al.* 1996, 1997; Hurwitz and Susswein, 1996) and the activity patterns and transmitters of the motor neurons controlling the buccal mass (Jordan *et al.* 1993; Morton and Chiel, 1993; Church and Lloyd, 1994). In addition, the feeding behavior of *Aplysia* species is modified by associative learning: animals can learn to associate particular tastes and textures with inedible food (Susswein *et al.* 1986; Chiel and Susswein, 1993).

Our previous work also suggests that it will be possible to analyze the biomechanics of the buccal mass. Earlier anatomical studies of the buccal mass indicated that it is composed primarily of muscle and cartilage (Eales, 1921; Howells, 1942; Starmühlner, 1956), with a relatively small internal vascular system (Drushel *et al.* 1993), and thus is a good model system for the study of a muscular hydrostatic system. By analyzing video tapes of small, transilluminated *Aplysia californica* that were engaged in swallowing and tearing movements, we were able to describe the *in vivo* kinematics of the buccal mass in intact animals (Drushel *et al.* 1997). We found that the buccal mass undergoes a series of characteristic shape changes during feeding movements. The overall shape changes can be used to infer the shape and positions of structures internal to the buccal mass, the radula and odontophore, which are used for grasping, tearing and ingesting food. Because there were no external markers on the buccal masses of these intact animals, we could not directly describe the kinematics of individual buccal muscles.

In the present study, we develop kinematic models to predict the location of specific structures within the buccal mass. Model assumptions about radular position and predictions of changes in the antero-posterior length of the buccal mass were tested using measurements of *in vivo* swallowing and tearing movements. An *in vitro* preparation was used to check the model's prediction about the location of the lateral groove. Having validated these predictions, we used these models to predict the kinematics of two superficial muscles of the buccal mass, I1 and I2. The I1 and I2 muscles are thin muscles whose borders can be inferred from a kinematic model that predicts the location of the border between them, the lateral groove (see Fig. 1A).

Portions of this work have appeared in preliminary form (Neustadter *et al.* 1992; Drushel *et al.* 1994).

Materials and methods

Kinematic models

In each kinematic model, there was one independent kinematic variable. Once it had been set, the geometrical constraints upon the structures determined their positions. We will describe the anatomical features of the buccal mass which were captured by each kinematic model, how these features were represented in each model, the anatomical basis of the model parameters and the algorithms used to calculate the positions of the structures given the value of the independent variable.

First kinematic model

Key anatomical features of the buccal mass

Our first kinematic model was designed to be simple enough that it could be rapidly simulated, and it made the assumption that the radula/odontophore complex does not change shape throughout the feeding cycle. A cutaway view of the *Aplysia californica* buccal mass (Fig. 1B) shows the features that were captured by the first kinematic model. In the resting, anesthetized buccal mass, the radula/odontophore complex is roughly spherical in shape. The muscles surrounding the radula/odontophore can be separated into two compartments, the most anterior of which consists of the jaw cartilages, the large circular bands of the I3 muscle, and the thin, fan-shaped superficial I1 muscle (Fig. 1A,B). The border of the anterior compartment is the lateral groove (Fig. 1A). One of the main muscles of the odontophore, the I4 muscle, interdigitates its fibers with the I3 muscle bands ventrally, forming a 'hinge' about which the radula/odontophore complex must pivot. The more posterior compartment of muscle surrounding the radula/odontophore consists of the thin, hemispherical I2 muscle and the esophagus. The dorsal surface of the esophagus is continuous with the pharyngeal tissues of the dorsal surface of the buccal mass, and the ventral surface is continuous with the posterior margin of the radula.

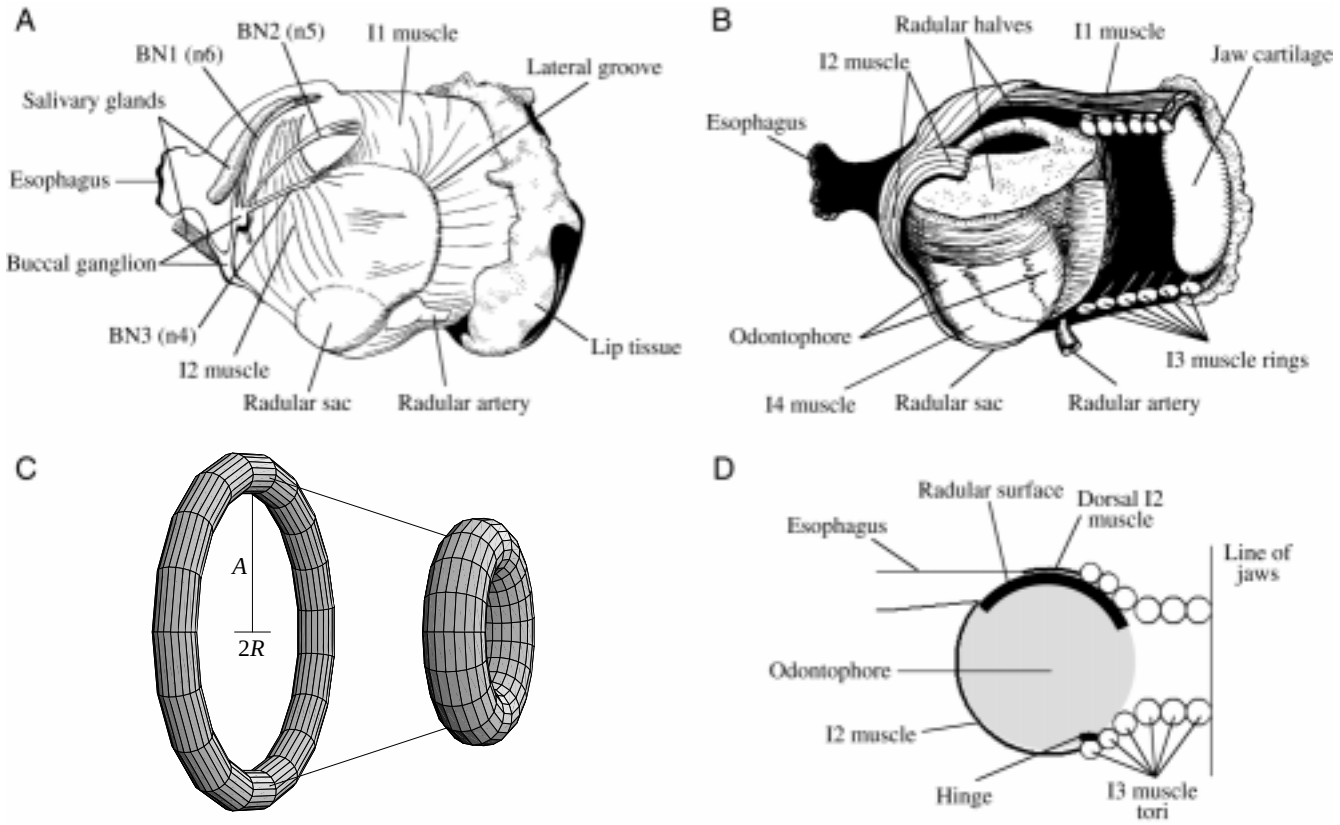

Fig. 1. Buccal mass anatomy and the first kinematic model. (A) Right lateral and slightly ventral view of the surface anatomy of the buccal mass of *Aplysia californica* (modified from Fig. 1 in Hurwitz *et al.* 1996). (B) Simplified cutaway view of the buccal mass, revealing the radula, odontophore and jaw cartilage. (C) Hydrostatic kinematic constraints on the I3 muscle bands. A change in the diameter of the torus leads to a compensatory change in its cross-sectional thickness to maintain a constant volume. The left torus has an annular radius A of 8 and a cross-sectional radius R of 1; the right torus has an annular radius of 4 and a cross-sectional radius of $\sqrt{2}$. Since the volume of a torus is $2\pi^2R^2A$, the two tori have the same volume. (D) Placement of radula/odontophore, I1/I3 bands and muscle I2 in the first kinematic model based on a simplified view of the anatomy (compare with B; for details, see Materials and methods).

Model components

These anatomical features were represented by the following elements of the model (Fig. 1D). (1) The radula/odontophore complex was assumed to be a sphere whose shape did not deform. The surface of the radula occupied a fixed location on the surface of this sphere relative to the hinge. (2) The I3 muscle was assumed to consist of six tori (doughnut-shaped rings), which were constrained to maintain a constant volume as any of their linear dimensions varied and to maintain a circular cross-sectional shape. For example, if a torus increased in its annular radius, its cross-sectional diameter decreased so that its volume remained constant (Fig. 1C). The I1 muscle was assumed to lie exterior to these tori, but was not explicitly represented. The surface of the most anterior torus was continuous with the outer jaws of the animal. The hinge point was located at the point of contact between the spherical radula/odontophore and the posterior I3 torus. The radular surface was at a fixed angle relative to the hinge (the arc representing the radula was drawn from the center of the circle from 90 ° to 200 ° counterclockwise relative to the location of the hinge). (3) The I2 muscle was assumed to be attached dorsally and ventrally to the most posterior I3 torus and to extend around the posterior side of the radula/odontophore. (4) The dorsal margin of the esophagus was assumed to be continuous with the most dorsal point of the structure, and the ventral margin was assumed to be continuous with the posterior edge of the radular surface.

Data for model parameters

The initial dimensions and placements of the elements of the kinematic model were based on digitized video pictures of buccal masses obtained from anesthetized animals (injected with an amount of isotonic 333 mmol l^{-1} $MgCl_2$ equal to half their body mass). Video tapes of the buccal mass were taken using a black-and-white video camera mounted on a dissecting microscope, and digitization was performed on a PC-based JAVA image processing system using a TARGA M8 imaging board (Jandel Scientific). The following measurements were used in the model: the diameter of the radula/odontophore complex, the thickness of the cut I3 muscle bands, the diameter of the front half of the buccal mass, and the distance from the jaws to the center of the odontophore.

Algorithm and simulation

The input to the algorithm for the first kinematic model was the distance of the spherical radula/odontophore from the line of the jaws, which was the fixed reference point for the model. Given the value of this independent kinematic variable, the algorithm placed the remaining structures around the sphere. The six tori of the I3 muscle were placed using an iterative algorithm. The first torus was placed along the line of the jaws at a radius slightly larger than that of the sphere, and its radius was then adjusted until it was either in contact with the sphere or at its rest radius (within a tolerance set by a minimum error value). Each subsequent torus was placed posterior to the previous I3 torus and was positioned such that it just contacted the band and either contacted the sphere or was at its rest radius (within the error tolerance), using an iterative bisection of its initial placement angle. Once the six tori had been placed, the I2 muscle was drawn around the posterior surface of the sphere, connecting the dorsal and ventral margins of the last I3 torus. The location of the hinge was determined by the contact point between the sphere and the posterior I3 torus, and this determined the location of the radular surface. Given the constraints described above, the lines representing the esophagus were then calculated.

As the sphere moved anteriorly from its initial, rest position (based upon the rest position of the jaws and radula/odontophore complex in the anesthetized buccal mass), the annular diameters assumed by the I3 tori when the radula/odontophore was not within their lumens were kept constant. In contrast, as the sphere moved posteriorly from its initial, rest position, the annular diameters of the I3 tori decreased linearly, allowing the cross-sectional diameters of the tori to increase so that the most posterior I3 torus remained in contact with the sphere.

The simulation of the model was written in Turbo C 3.0 for MS-DOS (Borland International). The compiled version runs in real time on a 486DX-33 computer. Computer code and QuickTime digital movies of the model output are available from the authors on request.

Second kinematic model

Additional anatomical features of the buccal mass

Comparisons of the shapes predicted by the first kinematic model with actual shapes of the buccal mass *in vivo* (Drushel *et al.* 1997) suggested that the changing internal shape of the radula/odontophore complex during the feeding cycle played an essential role in the overall shape of the buccal mass. We therefore developed a second, more computationally complex, kinematic model that captured additional anatomical features of the buccal mass. First, the radula/odontophore complex actually pivoted about the ‘hinge’ (the ventral attachment of the I4 and I3 muscles). This contrasts with the first kinematic model, in which the radula/odontophore was translated anteriorly or posteriorly, and the hinge location was determined by the placement of the I3 tori. Second, distinctive three-dimensional shapes for the radula/odontophore complex were used for the protraction, transition and retraction positions of the model. Third, constraints on the shapes of the I1/I3 muscles due to the jaw cartilages were incorporated.

Model components

The components of the second kinematic model are similar to those of the first kinematic model (Fig. 2D). (1) The radula/odontophore complex could be any arbitrary convex three-dimensional volume. The dimensions of any given volume were fixed. (2) The I3 muscle consisted of six rings that were constrained to maintain a constant volume as any of their linear dimensions varied and whose cross sections did not deform if they were in contact with the radula/odontophore. Their internal cavity was no longer circular, since the radula/odontophore was not assumed to be spherical, and instead was elliptical in quadrants to fit the region of the odontophore that they surrounded. The most posterior ring of the I3 muscle was connected to the base of the radula/odontophore by the hinge, and the radula/odontophore was pivoted about this fixed point. The I1 muscle was assumed to run exterior to the I3 muscle rings and was not explicitly represented in the model. (3) The I2 muscle was assumed to be a thin band of constant medio-lateral thickness, attached dorsally and ventrally to the most posterior I3 ring, and conforming exactly to the shape of the underlying radula/odontophore. The thickness of the I2 muscle was varied with I2 length to achieve a constant area of the two-dimensional mid-sagittal slice, in effect maintaining a constant volume for the muscle. (4) The cartilages of the jaw were represented as separate dorsal and ventral limits which constrained jaw closure to a mid-sagittal plane. Because there were no rigorous ventral landmarks to define its attachment to the buccal mass, the esophagus was not represented in this model.

Data for model parameters

As the radula/odontophore complex is deformed by the surrounding musculature, its passive properties could determine its overall shape and thus the shape of the whole buccal mass. These passive properties are due to the interdigitation of the I4 muscle fibers with cartilaginous tubes, the bolsters (Eales, 1921; Starmühlner, 1956), that significantly constrain the deformations of the muscle and thus of the odontophore as a whole. Three shapes of the radula/odontophore complex were therefore determined experimentally from fixed, dissected buccal masses: a rest shape, a protraction shape and a retraction shape. The rest shape was obtained by anesthetizing an animal with isotonic $MgCl_2$, dissecting out the buccal mass and fixing it in 10 % v/v formalin in isotonic $MgCl_2$, pH 7.5. The same fixation procedure was used for all the buccal mass shapes. The peak protraction shape was obtained by dissecting out a buccal mass from an anesthetized animal, compressing its posterior compartment, holding the radula/odontophore in the protracted position using dorsal and ventral metal clamps, and then fixing the tissue (Fig. 2A). The peak retraction shape was obtained

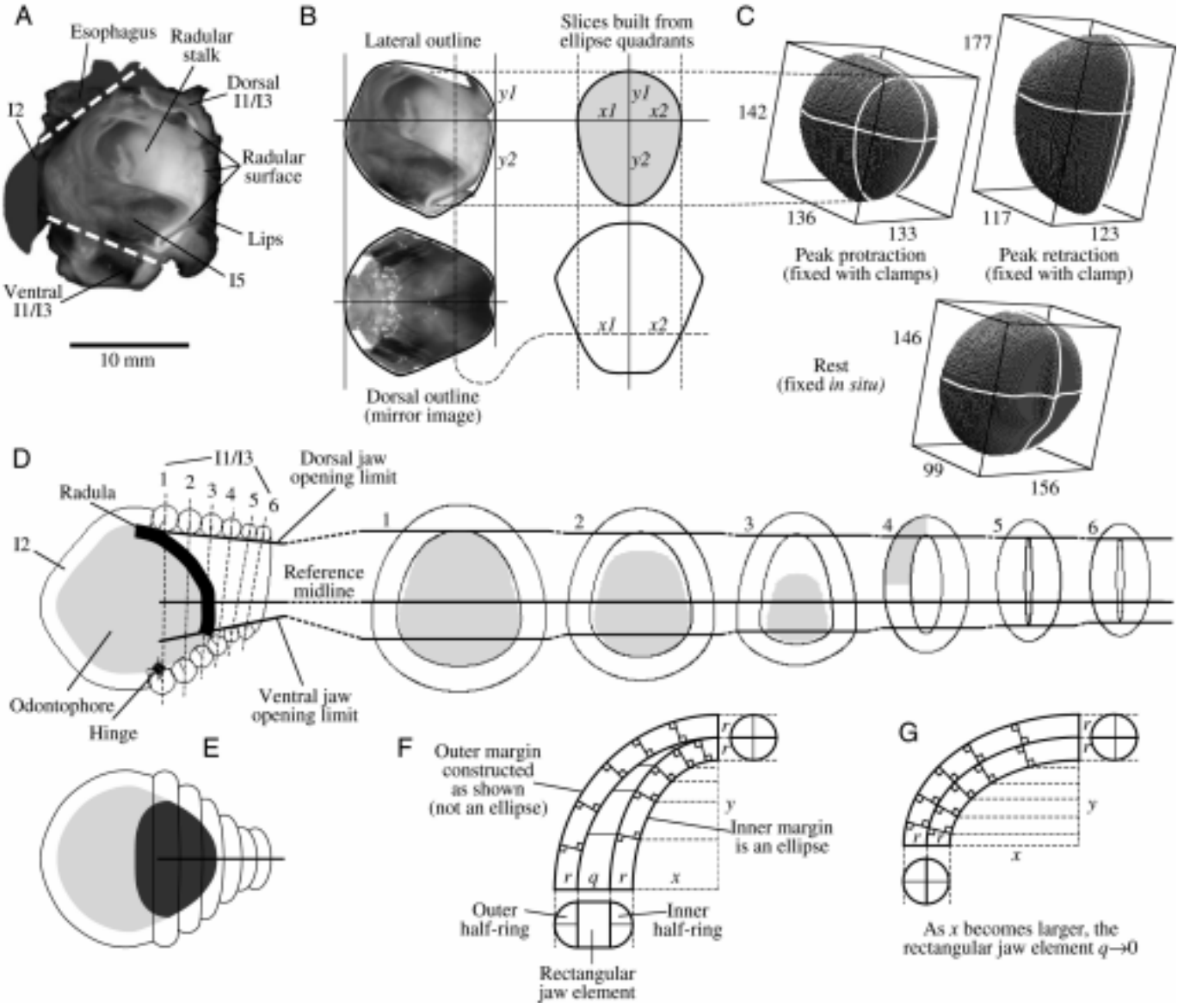

Fig. 2. Second kinematic model. (A) A fixed cross section of the radula/odontophore clamped into a protracted shape. The location of the clamps is indicated by the dashed lines. A retracted radula/odontophore was created with a single anterior clamp (not shown). A rest radula/odontophore was taken *in situ* from an unclamped, fixed buccal mass. (B) Construction of lateral and dorsal outlines (see Materials and methods). The solid line in the upper part of B defines the antero-posterior origin line at the widest dorso-ventral level of the lateral view, and *y1* and *y2* are the dorsal and ventral extent of the ellipses (broken lines). The origin line for the dorsal outline is indicated by the solid line at the midsagittal position, and the lateral extents of the ellipses are labeled *x1* and *x2*. (C) The resulting three-dimensional volumetric databases. The dimensions of each database in voxels are shown. All databases were normalized from their original construction dimensions to a constant volume. (D) The placement of I3 muscle rings relative to radula/odontophore shape. (E) Dorsal view of the model shown in D. (F,G) Detailed construction of the I3 rings (corresponding to the gray-shaded section in ring 4 of D). The inner margin (lumen) of each ring is an ellipse quadrant. Each ring consists of an inner and an outer half-ring (half a circle in cross section) plus a rectangular element *q*. For a given I3 ring, the *q* element is largest at the junction of the dorsal and ventral inner ellipse quadrants (i.e. the point of maximum lumen width) and decreases to zero dorsally and ventrally. Thus, the I3 ring is circular in cross section dorsally and ventrally, but a rounded rectangle laterally. The medio-lateral width of *q* varies inversely with the maximum width of the lumen such that, when the lumen is small (as the jaws 'close'), *q* is nonzero (F), and when the lumen is large (when the radula/odontophore is within the ring), *q* becomes zero and the I3 ring becomes circular in all cross sections (G). The I3 rings are constructed by erecting perpendiculars of length equal to the half-ring radius *r* from the inner ellipse; addition of the appropriate *q* values defines the inner margin of the outer half-ring, whose outer margin is also determined by erecting perpendiculars of length *r*. The final outer margin of the I3 ring is thus not an ellipse. The rationale for the introduction of the *q* element was to give a more realistic appearance to the I3 rings in frontal cross section at full jaw closure (see rings 5 and 6 in D). The volumes of the inner and outer rings and the *q* element are computed by separate numerical approximations and summed to give the final I3 ring volume. As in the first kinematic model (Fig. 1), the volume of each I3 ring was held constant through all changes in the lumen size over successive frames and in all model runs.

by dissecting out a buccal mass from an anesthetized animal, compressing its anterior compartment, holding the radula/odontophore in the retracted position using a single metal clamp at the lateral groove, and then fixing the tissue.

Three-dimensional volumetric databases for the model

Changing the shape of the radula/odontophore from a sphere to an arbitrary volume requires the creation of a database of three-dimensional points representing the surface of the volume. One possibility would be to use surface coordinates determined from a full three-dimensional anatomical reconstruction of fixed serially sectioned radula/odontophores. Instead, for computational ease and speed, we chose to approximate the surfaces of the fixed radula/odontophores using smooth ellipse quadrants for each section. The fixed buccal masses were cut in half along the mid-sagittal plane, and the medial surface was photographed. Fig. 2A shows the medial view of the buccal mass from which the protraction volumetric database was derived. One half of the radula/odontophore was dissected out, positioned such that its antero-posterior rotation was the same as in the undissected state, and photographed dorsally and medially. These two views of the dissected radula/odontophore were then used to construct a volumetric database (Fig. 2B). We approximated the radula/odontophore by successive slices composed of elliptical quadrants in frontal cross section. The lateral view of the radula/odontophore defined an antero-posterior origin line at the widest dorso-ventral level (solid horizontal line, top half of Fig. 2B), as well as the dorsal and ventral extents of the ellipses, relative to the origin line (labeled *y1* and *y2*, respectively, in the top half of Fig. 2B). The dorsal view of the radula/odontophore had its origin line at the midsagittal position (solid horizontal line, bottom half of Fig. 2B) and defined the lateral extents of the ellipses, relative to the midsagittal origin line (labeled *x1* and *x2* in the bottom half of Fig. 2B). Using the two origin lines and stepping from anterior to posterior, for each slice, smooth ellipse quadrants were drawn. Note that the dorso-lateral slice and antero-posterior slices derived from the lateral and dorsal outlines (shown on the right side of Fig. 2B) are represented as white outlines on the volumetric databases (Fig. 2C; the outlines shown in Fig. 2B were used to derive the peak protraction volumetric database). The rest and retraction volumetric databases were normalized to the protraction database volume by appropriate scaling of the lateral and dorsal outlines obtained from the dissections. Thus, a constant radula/odontophore volume was employed in all model runs.

Algorithm and simulation

The independent variable for the second kinematic model is the angle through which the three-dimensional radula/odontophore should pivot about the hinge. Given the value of this independent variable, and parameters describing the resting dimensions and volumes of the I1/I3 and the I2 muscles, the location of the hinge on the radula/odontophore surface, the location and dimensions of the jaw cartilages and the volumetric database representing the shape of the radula/odontophore, several algorithms position the remaining structures around the radula/odontophore. Both the volumetric database and its mid-sagittal outline are stored in arrays at 0 ° rotation, with the hinge location as the origin of the coordinate system for both. The mid-sagittal outline is rotated about the origin by the given angle, and the contact points for the I3 ring at the hinge are determined. The surface points on the mid-sagittal section are then mapped to surface points in the volumetric database coordinate system, and these points are used to generate a slice through the database at the correct angle. The ring is then fitted iteratively to this slice using elliptical quadrants, subject to the constraint that the ring should be in contact with the slice, within a minimal error tolerance, and have a fixed volume. More anterior rings are placed iteratively so that they are in contact with the previous ring and with the appropriate slice through the database, or with the dorsal and ventral jaw opening limits. The I2 muscle is then drawn around the posterior surface of the volumetric database, connecting the dorsal and ventral margins of the most posterior I3 ring (see Fig. 2D; lateral and frontal views of the six rings are shown, as well as the slice of the volumetric database that they surround; Fig. 2E shows a dorsal view). In some model simulations of peak retraction, the dorsal portion of the most posterior I3 ring was not in contact with the radula/odontophore. This case was handled by leaving the I2 muscle apposed to the radula/odontophore surface, but fixing its anterior extent by a perpendicular line through the center of the dorsal portion of the most posterior I3 ring. This was computationally simpler than modeling the I2 muscle pulled free of the surface of the radula/odontophore, and the error in the final I2 length was determined to be insignificant. As the rings of the I3 muscle are stretched over the volumetric database, their cross section is circular (Fig. 2G). However, as they close down over the dorsal and ventral jaw limits, a rectangular element is inserted between the inner and outer half ring so that the frontal profile is more similar to that of the jaw musculature observed *in vivo* (Fig. 2F, rings 4–6 in Fig. 2D). The element is constructed so that the isovolumetric constraint for the ring is maintained. The model generates lateral and dorsal views, as well as lists of the positions of each of its elements, and the perimeter of the I2 muscle in the mid-sagittal plane.

To show that the first kinematic model was a special case of the more general second kinematic model, we ran the second kinematic model using a spherical volumetric database and with no rectangular element inserted into the I3 rings. Under these conditions, the second kinematic model generated output identical to that of the first kinematic model (data not shown).

The model was implemented in Microsoft QuickBASIC 4.5 for MS-DOS with SVGA graphics and extended memory libraries (Zephyr Software). When run on a Pentium P100 computer under native MS-DOS, each rotational step of the model takes approximately 7 min. Computer code and QuickTime digital movies of model output are available from the authors on request.

Shape space analysis

In order to compare the shapes of the kinematic models in lateral view with those of the transilluminated buccal mass *in vivo*, we applied the analysis technique that was used for characterizing the shapes of the buccal mass during swallowing and tearing movements (Drushel *et al.* 1997). The lateral view produced by the kinematic model, like the lateral view of the actual buccal mass, can be approximated by four ellipse quadrants (Fig. 3A). Given antero-posterior axis lengths a and b (b is most anterior), and dorso-ventral axis lengths c and d (c is most dorsal), we define two shape parameters. The first shape parameter, *ellipticity*, is based upon the ratio of the two axes, $[(c+d)/(a+b)]-1$. When the axes are equal (i.e. when the shape is circular), the ellipticity is zero. An ellipse whose width is greater than its height has negative ellipticity, whereas its ellipticity is positive if its height is greater than its width. The second shape parameter, *eccentricity*, is based upon the fraction of the antero-posterior axis that lies anterior to the intersection of the two axes, $[b/(a+b)]-0.5$. Again, for a circle (whose axes intersect in the middle of the antero-posterior axis), the eccentricity is zero. A shape with its center skewed posteriorly ($b>a$) has positive eccentricity, whereas a shape with its center skewed anteriorly ($b<a$) has negative eccentricity. A plot of eccentricity *versus* ellipticity forms a two-dimensional region that we term *shape space* (Fig. 3C). Complex changes in shape translate into movements through different regions of shape space. The averaged buccal mass shapes observed during swallowing and tearing movements by Drushel *et al.* (1997) are shown in Fig. 3B, and their corresponding locations in shape space are shown in Fig. 3C. The gray region in Fig. 3C represents the averaged shape space locations assumed by the buccal mass during nine swallows and tears, corrected for the internal rotation of the buccal mass (data from Fig. 8 in Drushel *et al.* 1997).

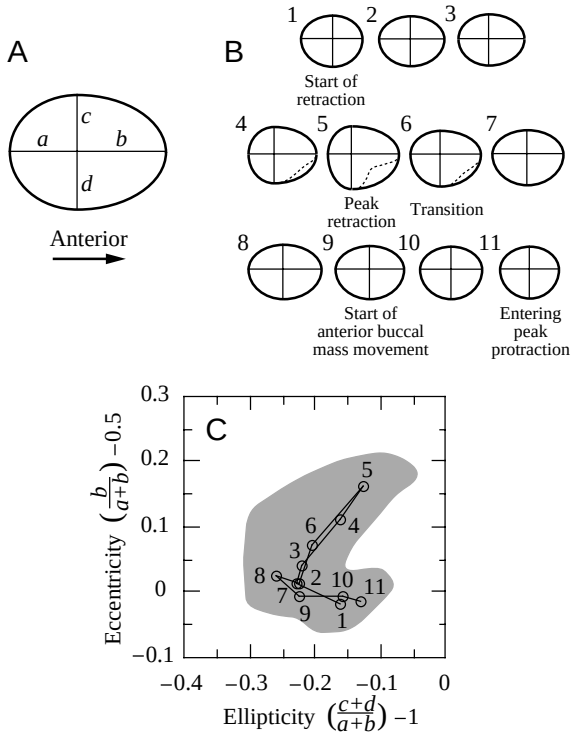

Fig. 3. Shape space analysis. (A) Definition of shape space parameters (see Materials and methods). (B) Representative shapes based on averaged *in vivo* data (from Drushel *et al.* 1997). Numbers refer to the numbered points in C. The dotted lines in shapes 4 to 6 represent the actual antero–ventral concavity of the buccal mass observed *in vivo*, which is not accurately represented by the ellipse quadrants. (C) Locations of these shapes in shape space; the gray outline shows the average shape space locations of the buccal mass *in vivo*, during the swallows and tears, corrected for the internal rotation of the buccal mass. Modified from Fig. 8 in Drushel *et al.* (1997).

Shape space analyses of the lateral views generated by both kinematic models were performed using the program developed for analysis of the buccal mass shapes observed *in vivo* (Drushel *et al.* 1997). Lateral views of the kinematic models were converted to solid black TIFF-format images and smoothed *via* a median filter of radius 15 pixels, using Adobe Photoshop 2.5.1 (Adobe Systems). This approximates the smoothing effect of transillumination *in vivo* as well as the resulting uncertainty in tracing transilluminated images. Smoothed model frames were analyzed by finding the bounding rectangle for the shape, giving the quantities $a+b$ and $c+d$. The division between a and b was set midway between the points of maximum convexity dorsally and ventrally. Similarly, the division between c and d was set midway between the points of maximum convexity posteriorly and anteriorly. This method gave good results even when shapes had slight concavities on one surface, giving two convexities instead of one.

All three volumetric databases were run through at least 90 ° of rotation, i.e. every model was run through a complete feeding cycle from peak retraction to peak protraction (based on radular position). Two criteria were used for determining a match between a model frame and *in vivo* kinematics: (1) the shape space coordinate (ellipticity, eccentricity) must fall within the *in vivo* shape space region (Fig. 3C); and (2) the model radular position must be relevant to the region of *in vivo* shape space being matched. Thus, a model frame whose shape space coordinate is consistent with peak retraction, but whose radular position is protracted, was not considered a match to the *in vivo* kinematics.

Measurements of radula position relative to jaw positions in intact, behaving animals

Juvenile *Aplysia californica* (Cooper) (10–20 mm long, N=3) were obtained from the *Aplysia* Resource Facility at the University of Miami (Miami, Florida, USA). Animals were kept in small breeder nets suspended in a tank of aerated artificial sea water (Instant Ocean, Aquarium Systems, Mentor, Ohio, USA), at 15–20 °C, and fed daily on seaweed (*Gracilaria* sp., Marinus, Inc., Long Beach, California, USA, stored frozen until fed to the animals). Animals were deprived of food for

1–2 days before studies were carried out, and only animals showing vigorous responses to seaweed were used. The animals were allowed to hang with their ventral side up from the surface of a dish filled with artificial sea water, using surface tension as an attachment, so that their mouths were easily accessible. A 1 % (w/v) solution of Fast Green FCF (Sigma, St Louis, Missouri, USA) in *Aplysia* saline (450 mmol l^{-1} NaCl, 10 mmol l^{-1} KCl, 22 mmol l^{-1} $MgCl_2$, 33 mmol l^{-1} $MgSO_4$, 10 mmol l^{-1} $CaCl_2$, 10 mmol l^{-1} glucose, 10 mmol l^{-1} MOPS, pH 7.5), filtered through a 0.2 μm filter (Acrodisc, Gelman Sciences Inc., Ann Arbor, Michigan, USA) was injected into the animal's mouth using a glass micropipette positioned by micromanipulator. This was found preferentially to stain the radular surface and the jaw cartilages. The dish was placed on a white background and illuminated directly, and the animals were then fed with small strips of seaweed held in forceps, while their behavior was video-taped under a dissecting microscope. The Fast Green had no observable effects on feeding behavior or on the health of the animals. More than 100 swallowing or tearing responses were elicited. The response selected for analysis had the clearest view of the internal structures.

Measurement of I2 electromyographic activity, antero-posterior length and the location of the lateral groove in vitro

The buccal mass was dissected out of one adult, anesthetized *Aplysia californica* (250 g, obtained from Marinus, Long Beach, California, USA) along with the cerebral and buccal ganglia. Extracellular electrodes were implanted in the I2 muscle in order to record its electromyographic (EMG) activity and thus to verify the presence of protraction movements (Hurwitz *et al.* 1996). The electrodes were made from twisted pairs of insulated stainless-steel wire (2.54 μm in diameter, California Fine Wire, Grover Beach, California, USA; Morton and Chiel, 1993) hooked into the muscle and attached using a drop of Duro Quick Gel cyanoacrylate glue (Loctite Corp, Rocky Hill, Connecticut, USA). The buccal mass was placed ventral side up in a 15 ml dish containing artificial sea water. Sequences of retraction/protraction movements were induced by replacing half the liquid in the dish with a solution of dopamine hydrochloride (1 mmol l^{-1}) (Sigma) dissolved in artificial sea water (Teyke *et al.* 1993). The movements of the buccal mass were video-taped (30 frames s^{-1}), and the EMG activity of the I2 muscle was amplified (model 1700 AC amplifier, AM Systems, Everett, Washington, USA), sampled at 2 kHz and recorded using a PC-based data-acquisition system (Axotape, Axon Instruments, Foster City, California, USA).

Estimating I1 and I2 lengths in vivo

As described in our previous paper (Drushel *et al.* 1997), the first four of the nine *in vivo* movements we describe were clearly swallows, since we observed seaweed moving into the buccal mass, and the last five were swallows/tears, since the seaweed moved inwards and chunks of seaweed were observed moving down the animal's esophagus. The nine cycles examined by Drushel *et al.* (1997) and in the present study were those in which both the dorsal and lateral views of the buccal mass were free of parallax, and they were selected from observations of more than 2300 swallowing and tearing responses in 25 *Aplysia californica* (for details of the apparatus and measurements in the transilluminated animals, see Drushel *et al.* 1997).

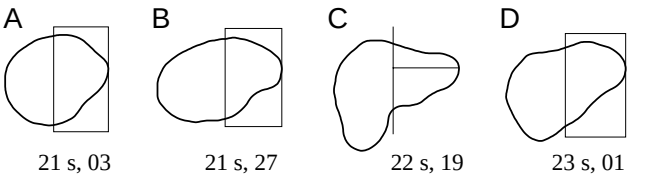

Fig. 4. Determination of I1 and I2 lengths from lateral *in vivo* views of buccal mass shape using the second kinematic model. Time in seconds, and frame number within that second (30 frames s^{-1}) are indicated beneath each outline. The width of the boxes in A, B, D indicate the length of the anterior compartment of the buccal mass, estimated from the second kinematic model as a percentage of total antero–posterior length. Thus, the left vertical edge of the box indicates the estimated location of the lateral groove. (A) Estimated border of I1 and I2 on an outline of buccal mass when the radula/odontophore is fully protracted (beginning of time interval *t1*; see legend of Fig. 9 for a definition of time intervals). (B) Estimated borders of I1 and I2 on an outline of buccal mass when the radula/odontophore is between protraction and retraction (transition, middle of time interval *t1*). (C) Estimated borders of I1 and I2 on an outline of buccal mass when the radula/odontophore is fully retracted (end of time interval *t1*). Note that the border, i.e. the lateral groove (indicated by a vertical line) is estimated on the basis of the external anatomy of the outline, since no kinematic model reproduced this shape exactly. This shape is referred to as the Γ (gamma) shape. (D) Estimated borders of I1 and I2 on an outline of buccal mass when the radula/odontophore is moving out of full retraction (end of time interval *t2*, peak retraction to loss of the Γ shape seen in C).

In order to estimate the lengths of the I1 and I2 muscles *in vivo* using the lateral views of the buccal mass during swallowing and tearing movements (Drushel *et al.* 1997), it was necessary to define the location of the lateral groove, which is the border between these muscles (Fig. 1A). Because the lateral groove is not visible in these views, the second kinematic model was used to estimate its location. The shape space characteristics of *in vivo* lateral views were matched to the lateral views produced by the second kinematic model, and the model then predicted the location of the lateral groove as a percentage of total antero-posterior length. Outlines of the *in vivo* shapes were divided at this percentage of their antero-posterior length (Fig. 4A,B,D). The perimeter of the posterior part of the outline was measured and used as an estimate of the length of the I2 muscle. The perimeter of the anterior part of the outline was also measured. All perimeter measurements were performed using the autotrace features of Canvas 3.5.3 (Deneba Software). The diameter of the seaweed held between the jaws (measured from the original video recordings) was subtracted from the perimeter of the anterior outline. The

remaining length of the perimeter was then halved to yield an estimate of I1 muscle length. Because the second kinematic model, given the volumetric databases, did not generate the shapes seen in full retraction, the border of the I1 and I2 muscles was estimated from the clearly visible location of the lateral groove on the *in vivo* profiles (Fig. 4C).

Results

Predictions of the first kinematic model

The model predicts that the overall antero-posterior length of the buccal mass shortens during protraction and lengthens during retraction (Fig. 5A). Furthermore, as the radula/odontophore complex moves posteriorly, the radular surface also rotates posteriorly and the esophagus opens (Fig. 5A, frame 0). As the radula/odontophore complex moves anteriorly, the esophagus closes, the radular surface rotates anteriorly and ultimately protracts through the jaws (Fig. 5A, frame 108). The position of the radular surface in peak protraction observed in an intact animal (Fig. 5B) is similar to that shown by the model (Fig. 5A, frame 108). The model predicts that the radula rotates through an angle of 90° as the odontophore moves from full retraction to its rest position, and rotates through another 90° as the odontophore moves into peak protraction. There is an inverse linear relationship between radula/odontophore position and radular rotation angle (Fig. 5C).

In full retraction, the model predicts that the I1 and I2 muscles are longer, and that the I3 muscle bands have smaller annular radii and thicker cross sections, than at rest (Fig. 5A, compare frames 0 and 55). In peak protraction, the model predicts that the I1 and I2 muscles are shorter, and that the I3 muscle bands have larger annular radii and thinner cross sections, than at rest (Fig. 5A, compare frames 55 and 108).

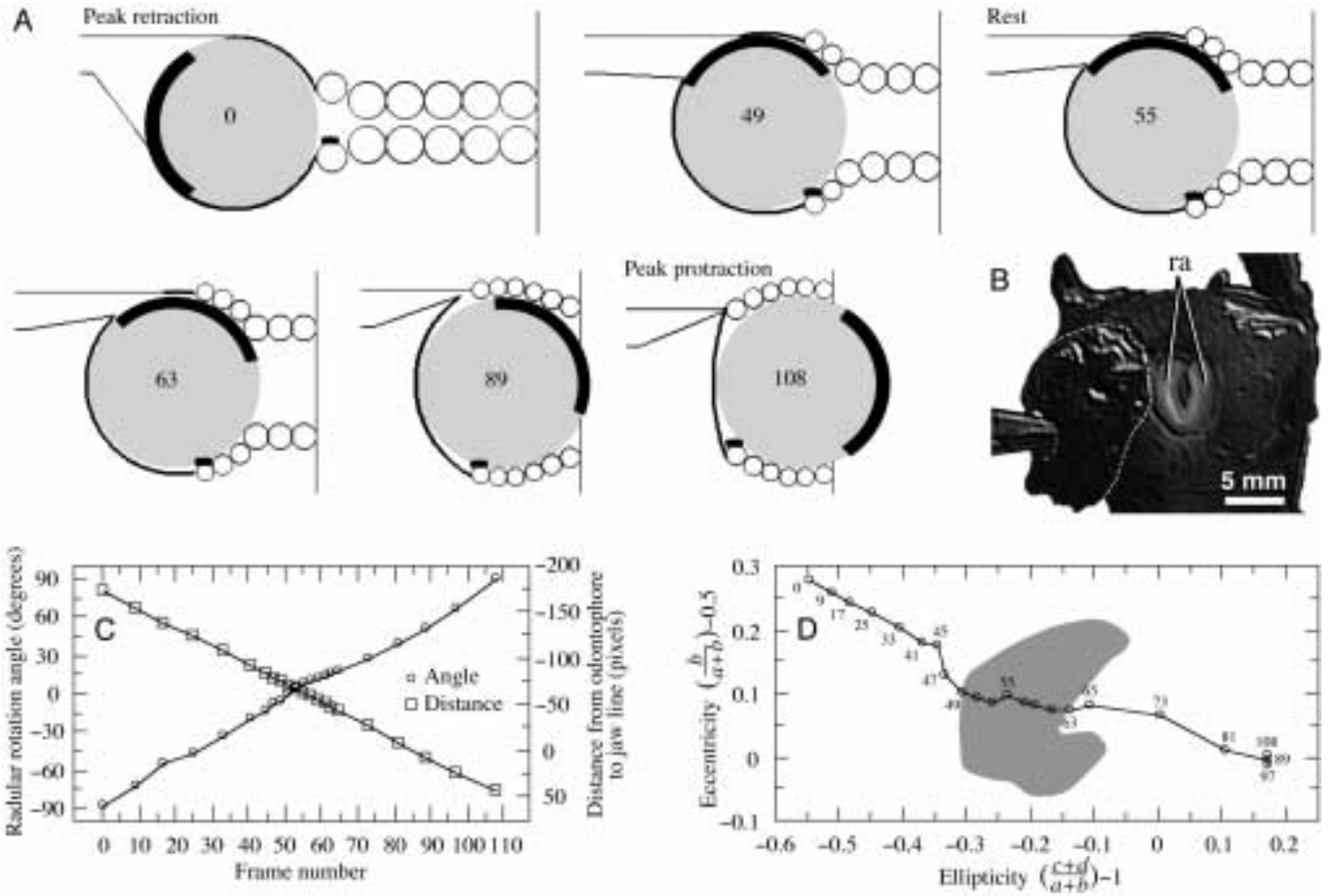

Fig. 5. Lateral views of the first kinematic model, predictions of radular position and overall buccal mass shape, and comparison with *in vivo* data. (A) Lateral views of the model as the radula/odontophore is moved from a fully retracted to a fully protracted position. Frame numbers are given within each view. (B) View of the fully protracted radula (ra) in an intact animal. The dashed line delimits the seaweed (held by forceps) used to induce feeding responses. Scale bar, 5 mm. (C) Radular rotation angle and the distance from the anterior margin of the odontophore to the jaw line as a function of steady translation of the radula/odontophore complex relative to the line of the jaws. Measurements were made from images of the model frames. (D) Shape space analysis of the first kinematic model (line) compared with the *in vivo* shape space region (gray area; taken from Drushel *et al.* 1997). The frame number for each point is indicated. Note that frames 89–108 have virtually the same shape space coordinates, even though the radula rotates by nearly 45° over this interval. Variables *a–d* are defined in Fig. 3.

To determine whether the kinematic model captured the overall shapes assumed by the buccal mass during swallowing and tearing, we performed shape space analyses on the lateral views generated by the model and superimposed them on the actual region in shape space occupied by the buccal mass *in vivo*. The model showed some correspondence to the *in vivo* shapes during protraction, but did not correspond well to shapes observed during retraction (Fig. 5D). These results suggested that changes in the shape of the radula/odontophore during the feeding cycle must be incorporated into the model in order to predict the overall shape of the buccal mass. This observation impelled us to construct the second kinematic model. Despite this serious limitation, the first kinematic model provided qualitative insight into the positions of structures within the buccal mass throughout the entire feeding cycle.

Predictions of the second kinematic model

The second kinematic model generated lateral views of the buccal mass whose shape space locations fell within the regions defined by the shapes of the buccal mass *in vivo* during swallowing and tearing movements (Fig. 6H). In addition, we used the dorsal views of the *in vivo* buccal mass (see Fig. 3 in Drushel *et al.* 1997) to evaluate the accuracy of the model. We found that the 'retraction' volumetric database generated buccal mass shapes that matched *in vivo* retraction shapes both laterally (Fig. 6A–C; note corresponding points in Fig. 6H) and dorsally, and that the 'protraction' volumetric database generated buccal mass shapes that matched *in vivo* rest and protraction shapes laterally (Fig. 6D–G; note corresponding points in Fig. 6H) and dorsally. Interestingly, the shape obtained from fixation in the anesthetized 'rest' position was too wide in dorsal view and thus did not appear to fit accurately any of the observed shapes *in vivo* (data not shown). The results from the first and second kinematic models support the inference, based on observations of the shape changes of the buccal mass *in vivo* (Fig. 10 in Drushel *et al.* 1997), that the changes in the shape of the radula/odontophore complex play an important role in determining overall buccal mass shape during the feeding cycle. Indeed, if the 'retraction' and 'protraction' volumetric databases were rotated through the entire range of rotation of the buccal mass, neither of them was capable of generating lateral or dorsal views that fitted the entire range of shapes observed *in vivo* (data not shown). Also note that, with the given volumetric databases, we were unable to match the full retraction shapes (Fig. 3C, points 4 and 5; Fig. 4C), suggesting that the active movements of the radula/odontophore complex may play an important role in generating these shapes.

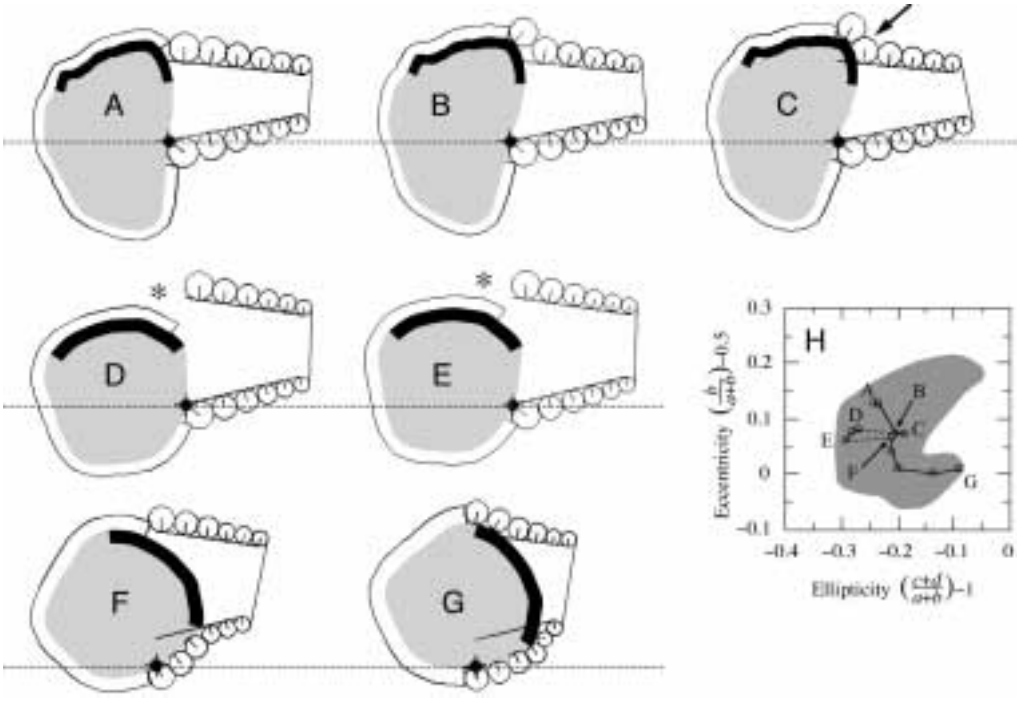

Fig. 6. Lateral views of the second kinematic model, its predictions of radular position and overall buccal mass shape and comparison with *in vivo* shape space data. All views are aligned by the location of the hinge (dashed line). (A–G) Representative model runs. A–C use the peak retraction volumetric database, rotated about the hinge at angles of +5°, +10° and +20°, respectively. The arrow in C indicates a small failure of the I3 ring-fitting algorithm at the corner formed by the dorsal jaw limit line and the radula/odontophore surface; the effect on shape space parameters is insignificant. D–G use the peak protraction volumetric database, rotated about the hinge at angles of −120°, −110°, −70° and −50°, respectively. Asterisks in D and E show the behavior of the I2 fitting algorithm when the first dorsal I3 ring is not in contact with the radula/odontophore surface (see Materials and methods). (H) Shape space plots of A–G. Sequential rotational steps (in 5° increments) are connected with solid lines; breaks between different model runs/parameter sets are shown with dashed lines. The gray region is that bounding the nine *in vivo* swallows and tears analyzed in Drushel *et al.* (1997). Variables *a–d* are defined in Fig. 3. Note that D–E and F–G are two different model runs, with two slightly different parameter sets. The dorsal and ventral jaw limit lines are translated upwards by 5 model units in F–G compared with D–E. This has the effect of keeping the radular surface centered in the jaw cavity as peak protraction is approached. The slopes of the jaw limit lines, as well as the volumetric database and the location of the hinge point upon its surface, are the same in both model runs. For the retraction model runs (A–C), a third set of jaw limit line slopes and *y*-intercepts was used. The limits have a shallower slope and are closer together. This approximates the appearance of *in vivo* peak retraction (Fig. 4C; also compare first kinematic model frame 0, Fig. 5A).

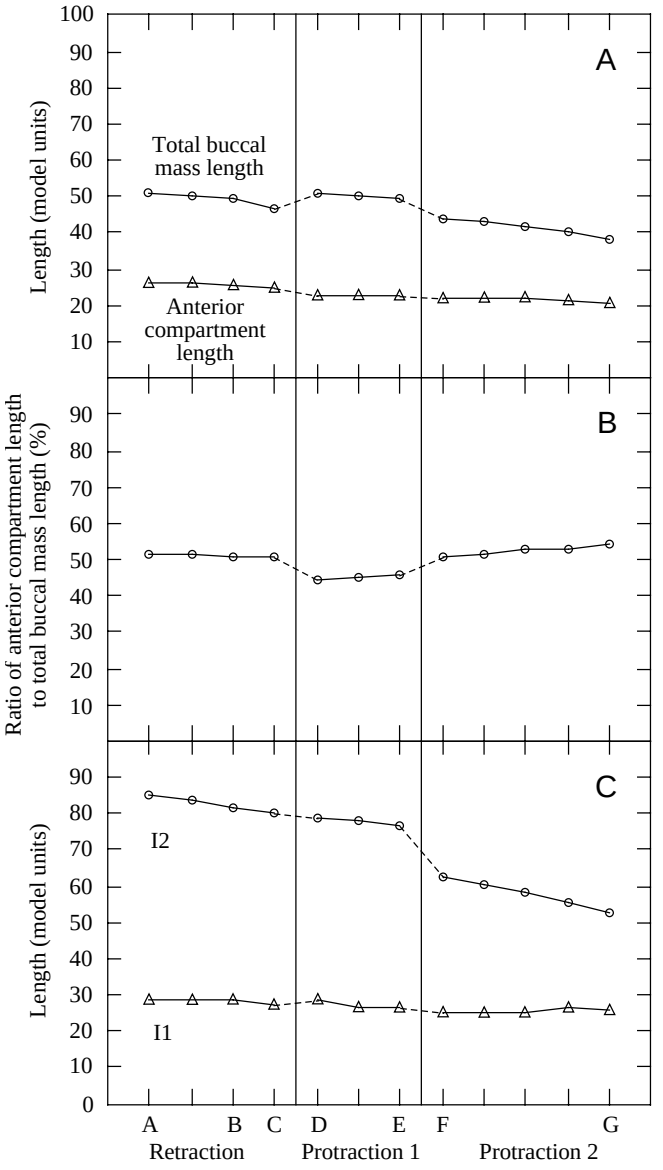

Fig. 7. Predictions of the second kinematic model during a feeding cycle. (A) Predicted total antero-posterior length of the buccal mass (circles) and predicted length of the anterior compartment (distance from lateral groove to anterior tip of buccal mass; triangles). (B) Predicted ratio of anterior compartment length to antero-posterior length expressed as a percentage. (C) Predicted length of I1 (triangles) and I2 (circles). Points corresponding to model frames shown in Fig. 6A–G are indicated at the bottom of the graph. The angular rotation values for each database are relative to the zero point for the particular volumetric database, which is defined as the radula/odontophore position in the original fixed buccal mass when the buccal mass angle was 0 ° (i.e. when a line through the jaws and esophagus was horizontal). Thus, between volumetric databases, a given angle does not represent the same radular position. For example, the radula points dorsally in the retraction database at 0 ° but anteriorly in the protraction database at 0 °. Owing to uncertainty of shape changes, no attempt was made to normalize the rotations on the basis of absolute radular position. The angles used for the retraction database were +5 °, +10 °, +15 ° and +20 °. The angles used for the protraction database with the first set of hinge and jaw line parameters (protraction 1) were −120 °, −115 ° and −110 °. The angles used for the protraction database with the second set of hinge and jaw line parameters (protraction 2) were −70 °, −65 °, −60 °, −55 ° and −50 °.

Because the second kinematic model was able to match the overall *in vivo* buccal mass shapes more accurately, we used it to predict several features of the buccal mass during the feeding cycle (Fig. 7). The second kinematic model predicts that total antero-posterior buccal mass length will decrease by 25 % from its maximum length in retraction to its minimum length in protraction (all percentage changes are scaled relative to the maximum value). The distance from the border of the I1/I2 muscles (i.e. the equivalent of the lateral groove) to the anterior tip of the buccal mass (defined as the anterior compartment length) decreases by 23 % from its maximum in retraction to protraction (Fig. 7A). The similar percentage changes in length imply that the ratio of the anterior compartment length to the total antero-posterior length of the buccal mass should be essentially unchanged. In fact, the predicted ratio is very close to 50 %, ranging from 45 to 53 % (Fig. 7B). The estimated length of the I1 muscle decreased by 13 % from its maximum length, suggesting that its length does not change greatly during the feeding cycle. The estimated length of the I2 muscle decreased by 38 % from its maximum length in retraction to its minimum length in protraction (Fig. 7C).

Since the second kinematic model does generate shapes similar to those observed *in vivo*, we sought to test the accuracy of its predictions. We therefore performed experimental studies (1) to test its assumptions about the movements of the radula during the feeding cycle, and (2) to test its predictions about changes in the antero-posterior length of the entire buccal mass during swallowing and tearing movements, and the relative position of the lateral groove. After validating these assumptions and predictions, we used the model to estimate the changes in the length of the I1 and I2 muscles during these behaviors.

Changes in radular position in vivo

Both kinematic models implicitly assumed that the radula surface rotates anteriorly in protraction and posteriorly in retraction. What positions does the radular surface assume during a normal feeding cycle? The radular position is clearly visible in directly illuminated juveniles after staining with Fast Green (see Materials and methods). During swallowing, at the peak of protraction (Fig. 8A,D,G), the radular surface is pressed up against the cartilage of the jaws. At the peak of retraction, the radular surface rotates posteriorly and opens near the entrance of the esophagus (Fig. 8B,E,H). At rest (Fig. 8C,F,I), the radular surface points dorsally, perhaps inclined slightly posteriorly.

Changes in antero-posterior length of the buccal mass in vivo

How does the antero-posterior length of the buccal mass

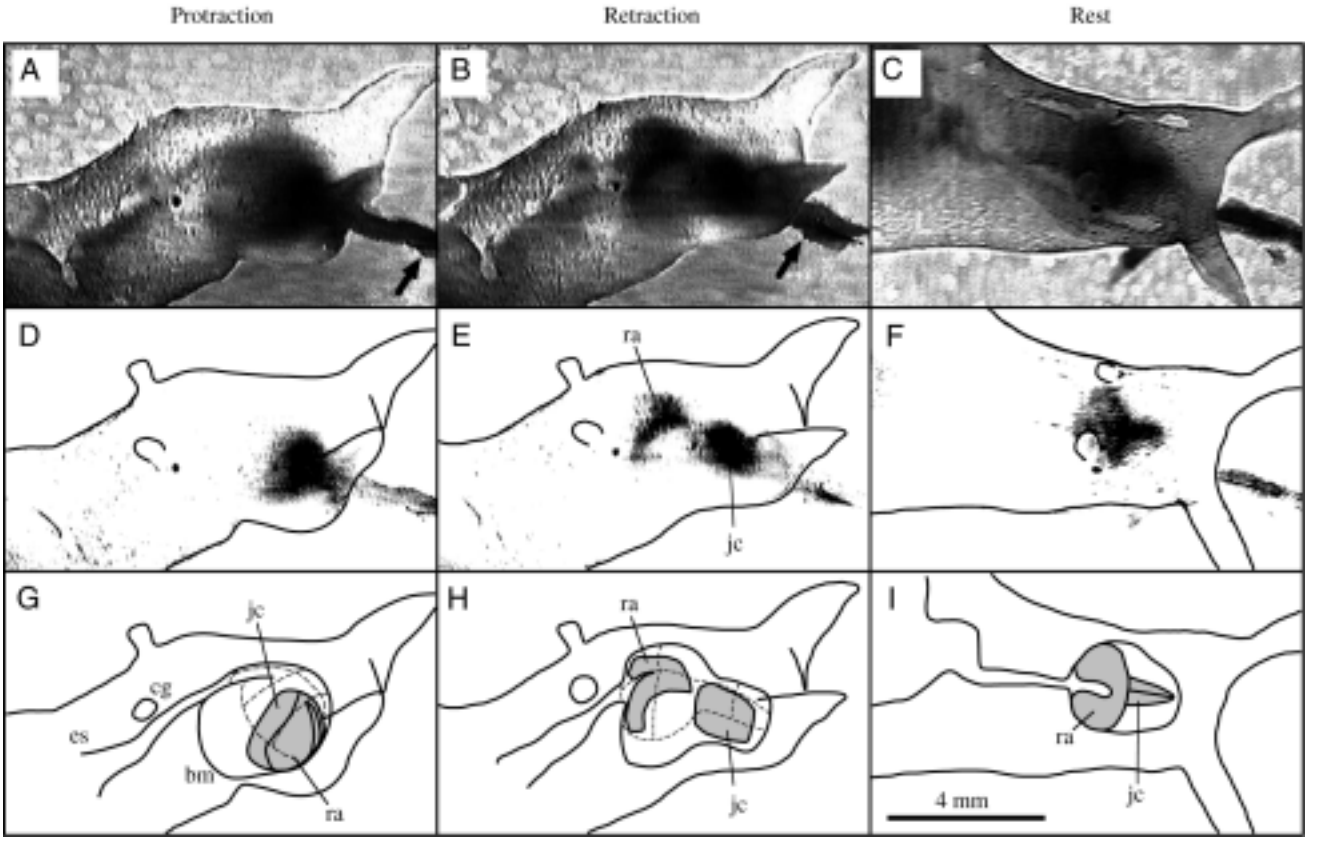

Fig. 8. Changes in radular position during feeding and at rest. (A–C) Grayscale video frames (from 24-bit RGB color originals of a directly illuminated 15 mm *Aplysia californica* swallowing a cut stipe of *Gracilaria*), corresponding to protraction, retraction and rest, respectively. A and B are lateral views from a single swallowing event; C is a dorsal view when the animal is aroused but is not actively feeding (the seaweed is not in the animal's jaws). The radula and jaw cartilages of the animal have been stained using Fast Green and, while vividly distinct in the original color video, are obscured in grayscale by the buccal mass. Arrows in A and B indicate the same point on the seaweed, which moves inwards by 1.45 mm between A and B. (D–F) Line drawing of the outline of animal's head superimposed on stained portions of its anatomy which have been extracted using contrast enhancement and filtering procedures in Adobe Photoshop 2.5.1. D, E and F correspond to A, B and C, respectively. (G–I). Line drawings based on repeated viewing of video tape and filtered stained regions. The radular surface is close to the jaws in the protraction phase of swallowing, is close to the opening of the esophagus in full retraction and is at an intermediate position during rest. Compare with Figs 5 and 6. ra, radula; jc, jaw cartilages; cg, cerebral ganglion; es, esophagus; bm, buccal mass. Scale bar, 4 mm.

change during feeding? To test the predictions of the second kinematic model, we analyzed the antero-posterior lengths of lateral views of small, transilluminated animals as they engaged in swallowing and tearing movements (Fig. 9). These were the same lateral views whose eccentricity, ellipticity and shape space locations were extensively analyzed in our previous study (Drushel *et al.* 1997). Over the course of the nine behavioral responses, several consistent phenomena were noted. First, the overall percentage change in the antero-posterior buccal mass length from its maximum to its minimum value was 22±2.4 % (mean ± S.D., N=9 cycles), which is quite similar to the 25 % length change predicted by the second kinematic model. Second, the minimum antero-posterior buccal mass length for all nine responses occurred at the peak of protraction (border between the intervals *t4* and *t1*; see legend to Fig. 9 for definitions of *t1–t4*), which was also consistent with the prediction of the second kinematic model. Third, in seven of the nine responses (excluding responses 4 and 9 in Fig. 9), the maximum antero-posterior length occurred after the loss of the Γ-shape (this shape is shown in Fig. 4C; referred to as shape 3 in Drushel *et al.* 1997) and the beginning of anterior buccal mass movement (i.e. at the end of interval *t3*), rather than at the presumed peak of retraction (end of interval *t1*), which was the time of peak antero-posterior length predicted by the model.

Position of the lateral groove in vitro

The second kinematic model predicts the relative position of the lateral groove throughout the feeding cycle. This prediction was tested by examining the actual position of the lateral groove in an isolated buccal mass undergoing sequential protraction–retraction sequences. Visual observation and measurement of the I2 EMG activity confirmed that applications of dopamine induced rhythmic protraction/retraction sequences in this preparation (Fig. 10B). The position of the radula/odontophore complex was inferred both

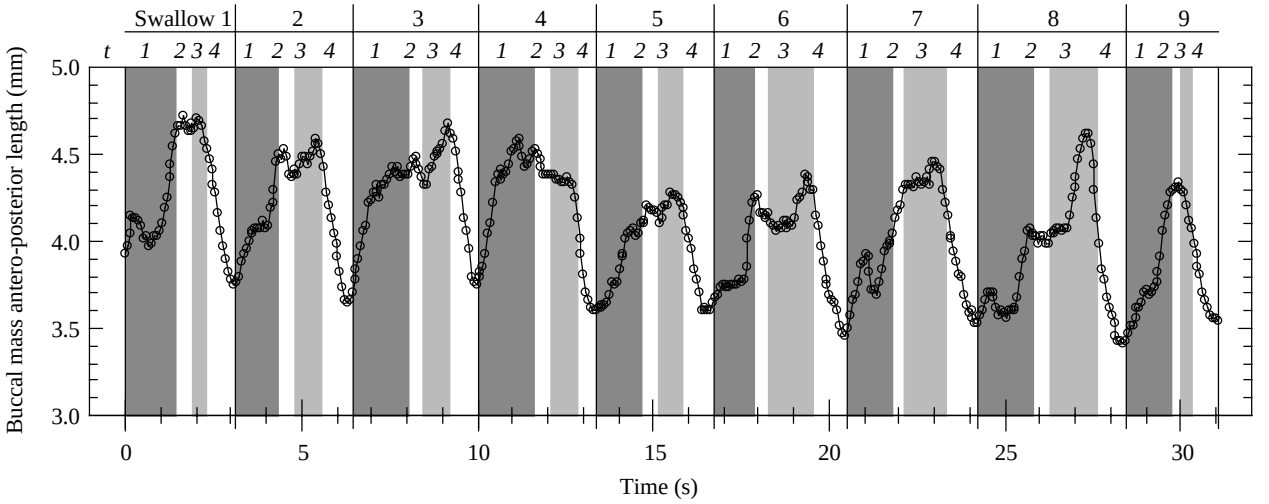

Fig. 9. Changes in buccal mass antero-posterior length measured from lateral views of transilluminated *Aplysia californica* during swallowing and tearing. Each swallow is delimited by a vertical line, and intervals *t1–t4* (see Drushel *et al.* 1997) are indicated by shaded regions. The intervals are defined as follows: *t1*, peak protraction to peak retraction; *t2*, peak retraction to the loss of the Γ shape (shape 3; Fig. 4C); *t3*, loss of shape 3 to the start of anterior buccal mass movement; *t4*, start of anterior buccal mass movement to peak protraction.

from the changing shape of the buccal mass and from the location of the radular stalk, which could be visualized directly through the thin I2 muscle. Unlike the movements observed *in vivo* during swallowing and tearing, the radula/odontophore never assumed the fully retracted Γ shape in which the base of the radular sac bulges ventrally through the posterior region of the I2 muscle (see Fig. 4C).

During retraction/protraction cycles *in vitro*, the overall antero-posterior length of the buccal mass changes rhythmically from a maximum length in retraction to a minimum length in protraction. The initial retraction-to-protraction movement causes a 27 % change in antero-posterior length, comparable to the change observed *in vivo* (Fig. 10A, circles). However, subsequent movements are associated with larger excursions in length, and percentage changes range from 39 to 53 %. Unlike the movements seen *in vivo* during swallowing and tearing, the antero-posterior length changes are smooth and fairly sinusoidal, and the peak length clearly occurs at the peak of retraction (compare Fig. 9; note that the beginning and end of the *t1* interval were determined from buccal mass movements, not from length measurements).

Since the underlying jaw cartilages provide some stiffness to the anterior compartment of the buccal mass, is the distance from the lateral groove to the anterior tip of the buccal mass fixed? The data from the *in vitro* preparation show that the distance from the lateral groove to the anterior tip of the buccal mass changes rhythmically (Fig. 10A, triangles). Interestingly, the percentage change varies much less than that observed for the antero-posterior buccal mass length, ranging from a minimum of 23 % to a maximum of 32 %. The first response is associated with the smallest percentage change in the anterior compartment length, 23 %, which is comparable to the value predicted by the second kinematic model.

Is the length of the anterior compartment a fixed, or nearly fixed, fraction of the total antero-posterior length? This would be consistent with the second kinematic model, which predicted that the fraction would vary between 45 and 53 % over the course of a feeding cycle (Fig. 7). *In vitro*, the percentage varies between 42 and 58 % over the course of the feeding-like cycle (Fig. 10C), which is in good agreement with the model. Again, the first response, in which the fraction varies from 42 to 51 %, is closest to the values predicted by the model.

Estimated I1 and I2 lengths in vivo

Since the assumptions and several predictions of the second kinematic model were validated by *in vivo* and *in vitro* measurements, we used the model to predict the kinematics of two intrinsic buccal muscles, I1 and I2. The second kinematic model provides an estimate of the location of the border between the I1 and I2 muscles, i.e. the lateral groove (Figs 1A, 2D). The shape space coordinates of every frame from the nine consecutive swallows recorded *in vivo* (Drushel *et al.* 1997) were compared against the coordinates of the second kinematic model frames that lay in functionally appropriate regions of shape space (Fig. 6H). Of a total of 467 frames, 99 (21 %) matched at least one of the model frames. The buccal mass outlines were divided into anterior and posterior compartments, using the ratio of anterior compartment length to total buccal mass length of the particular matching model frames (Fig. 4A,B,D). Because the borders of the anterior compartment were clearly visible in the *in vivo* lateral views near and at peak retraction, another 49 (10 %) *in vivo* outlines were divided into anterior and posterior compartments (Fig. 4C). The length of the posterior compartment outline was considered to represent the I2

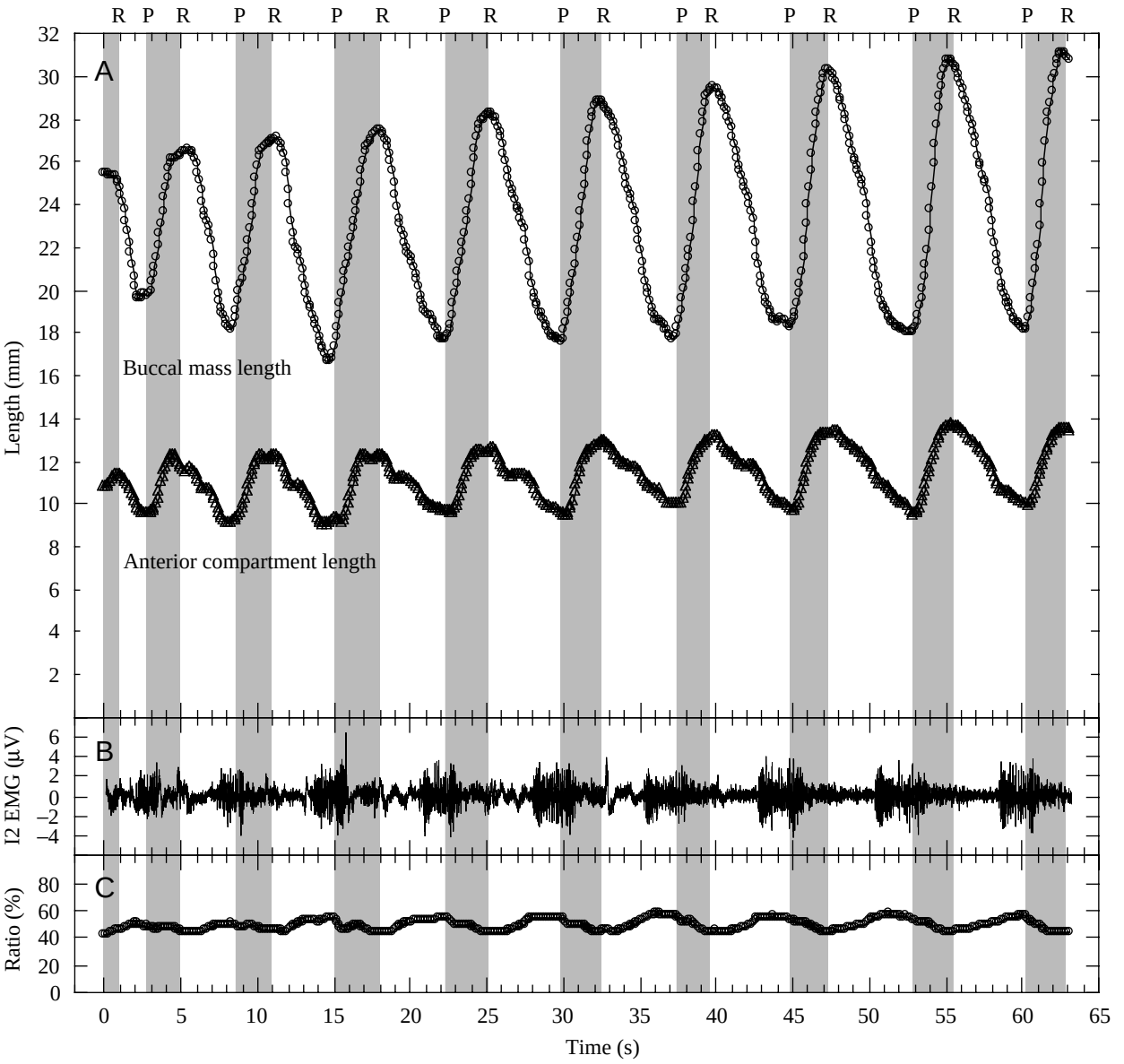

Fig. 10. Measures of the antero-posterior length of the buccal mass, the distance between the anterior tip of the buccal mass and the lateral groove (anterior compartment length) (A), I2 EMG activity (B) and the fractional position of the lateral groove (C) using an isolated buccal mass *in vitro*, stimulated with dopamine to produce rhythmic protractions and retractions. The I2 EMG activity shown in B is similar to that observed *in vivo* during feeding motor programs (Hurwitz *et al.* 1996). (C) The fractional position of the lateral groove (the ratio of data shown in the top and bottom traces of A at each time point). R, peak retraction; P, peak protraction. These peaks were determined by observing the overall movements of the buccal mass on video tape, not from the length measurements.

muscle length, that of the anterior compartment to represent slightly more than twice the average I1 length (see Materials and methods).

The estimated I1 muscle length changes from maximum to minimum (Fig. 11, filled circles) were 17.3±0.9 % (mean ± S.D., *N*=9 cycles), which is slightly larger than the 13 % change predicted by the second kinematic model. There was no consistent trend in the length changes of the I1 muscle during the feeding cycle, which was also similar to the predictions of the second kinematic model.

The estimated I2 length changes from maximum to minimum (Fig. 11, open circles) were 35±2.5 % (*N*=9 cycles), which compares favorably with the 38 % change from maximum to minimum length predicted by the second kinematic model. In general, the maximum I2 length occurs at the peak of retraction (end of interval *t1*) and the minimum I2 length occurs at the peak of protraction (beginning of interval *t1*), in accordance with the predictions of the model.

Discussion

We have created two kinematic models in order to

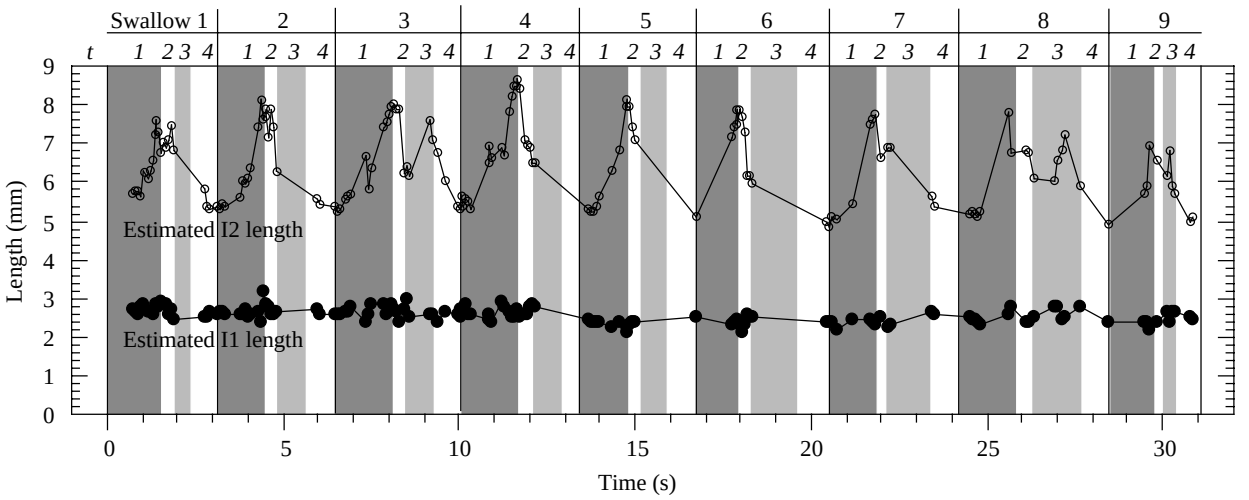

Fig. 11. Estimated lengths of I1 (filled circles) and I2 (open circles) *in vivo*. The shape space characteristics of outlines of the buccal mass *in vivo* were used to match them to specific configurations of the second kinematic model. The model predicts the location of the lateral groove dorsally and ventrally, which is the I1/I2 border. Arc lengths of I1 and I2 were then measured (see Materials and methods). The points shown are 32 % (148/467) of the total *in vivo* frames from the nine consecutive swallows (Drushel *et al.* 1997). Periods *t1–t4* are defined in Fig. 9.

characterize the movements of the structures within the buccal mass of *Aplysia californica* during feeding responses. Both kinematic models made specific predictions about the overall shape of the buccal mass and the positions of the superficial I1 and I2 muscles. Although the first kinematic model provided very useful qualitative insights into the overall behavior of the buccal mass, it did not accurately predict overall shapes for the buccal mass during retraction. We therefore constructed a second, more accurate, kinematic model, which did generate overall shapes that were similar to those observed *in vivo* during swallowing and tearing. The second kinematic model made predictions about the antero-posterior length of the buccal mass and the relative location of the lateral groove that were consistent with measurements of buccal mass properties both *in vivo* and *in vitro*, thus allowing us to estimate the kinematics of the intrinsic muscles I1 and I2 *in vivo*. We will discuss the limitations of these models, compare the model predictions with the data obtained *in vivo* and *in vitro*, and then use the models to make predictions about the neural control of the buccal mass.

Limitations of models

A fundamental limitation of both models presented in this paper is that they are kinematic rather than kinetic models. As a consequence, one cannot directly determine which structure exerts force on the others to generate the shapes and movements that are observed *in vivo*. In addition, because the model does not represent the forces generated by the muscles, it cannot be directly linked to a neural network controller. Despite these limitations, kinematic modeling is quite useful for formulating hypotheses about the likely functional role of the different muscles of the buccal mass (see below). Moreover, the kinematics predicted by the models and verified experimentally serve as an important constraint on any future kinetic model, because a correctly formulated kinetic model should generate these kinematics. Finally, the relative ease with which it is possible to construct and analyze a kinematic model is a significant advantage for permitting modeling and experimental studies to progress interactively.

A model of a biological structure is only as good as the assumptions and data underlying it. Several simplifying assumptions were made in order to construct the kinematic models. To construct the first kinematic model, we made the assumption that the radula/odontophore complex was spherical. This is clearly inaccurate. The advantage of this assumption was that it made it possible to calculate the output of the model rapidly, providing a useful animation of the movements that might underlie the protraction and retraction movements of the buccal mass. The model also made predictions about the overall shape of the buccal mass, and this impelled us to make a detailed study of the *in vivo* kinematics of the buccal mass (Drushel *et al.* 1997). The failure of the first kinematic model to match the shapes observed *in vivo* strongly contradicted the assumption that the changing, nonspherical shape of the radula/odontophore could be ignored in predicting overall buccal mass shape. This led us to examine the different shapes assumed by the radula/odontophore. No single fixed shape for the radula/odontophore could generate the full range of buccal mass shapes observed *in vivo*, and this led us to construct the second kinematic model using different shapes for different parts of the feeding cycle. Thus, the relative simplicity of the initial kinematic model provided very useful guidance for understanding the features that needed to be represented in order to capture the kinematics of the buccal mass more accurately and supported the hypothesis that the change in shape of the radula/odontophore throughout the feeding cycle

makes a major contribution to the overall shape of the buccal mass.

The second kinematic model also made several simplifying assumptions. First, we assumed that the passive properties of the radula/odontophore, after it was deformed by the surrounding tissues, would account for most of the shape of the entire buccal mass. Second, we did not make three-dimensional reconstructions of the actual fixed radula/odontophore, but chose to use ellipse quadrant approximations for building the volumetric databases. Discrepancies between the second kinematic model and the buccal mass shapes observed *in vivo* are probably due to the limitations of these assumptions. The peak retraction shape observed *in vivo* during swallowing and tearing (Fig. 4C) was not reproduced by rotations of any of the volumetric databases, suggesting that active contractions of the radula/odontophore play an important role in generating the peak retraction shape. The observation that the 'rest' database did not generate realistic shapes when its dorsal view was compared with those obtained *in vivo* suggests two possibilities, which are not mutually exclusive: (1) the process of fixation may deform the buccal mass significantly from a true 'rest' position; and (2) the 'transition' shape observed *in vivo* may be different from the 'rest' shape assumed after anesthetizing a buccal mass. The ability of the second kinematic model to reproduce the *in vivo* observations and to detect nonphysiological distortions in the 'rest' database suggests that detailed reconstructions of the actual three-dimensional anatomy of the radula/odontophore may not be necessary to gain useful insights into the overall shapes assumed by the buccal mass during feeding.

In both kinematic models, we assumed that none of the structures of the buccal mass was deformed by any other and that their volume was constant. Since the buccal mass is composed of muscle, cartilage and compressible vascular spaces, these assumptions are inaccurate. Structures within the buccal mass must continuously deform one another, and vascular spaces are also significantly deformed by contractions of surrounding muscles and their volume may change. It is therefore quite interesting that the second kinematic model quantitatively predicted properties of the buccal mass that were verified by both *in vivo* and *in vitro* measurements. This suggests that the mutual deformation of structures within the buccal mass can be captured to a first approximation by accurately representing the muscular hydrostatic properties of the I3 muscle bands and the internal shapes of the radula/odontophore. The constraints on deformation of the radula/odontophore are consistent with our observations that the I4 muscle, whose fibers interdigitate with cartilaginous bolsters (Eales, 1921; Starmühlner, 1956), is relatively difficult to deform. The assumption that the volume is constant is consistent with our observations that the vascular compartment of the buccal mass is relatively small (Drushel *et al.* 1993). Moreover, the radular surface and the cartilage of the jaws, as well as the muscular hydrostatic properties of muscle, impose significant constraints on the shapes that the buccal mass can assume. Thus, these simplifying assumptions capture many aspects of buccal mass behavior.

In order to relate neural control to muscle kinematics, it is essential to have a model that provides continuous kinematic information. A more realistic kinematic model of the radula/odontophore complex should generate a continuous range of internal three-dimensional shapes to which the surrounding I2 and I1/I3 muscles must conform, and this would provide a continuous match to the full range of buccal mass shapes seen *in vivo*. Moreover, it is likely to provide insight into the kinematics of other intrinsic buccal muscles, such as I4, I5, I6 and I7 (Howells, 1942; Scott *et al.* 1991). The kinematic models can then serve as the basis for constructing kinetic models that can directly predict the interactions between neural network control and peripheral biomechanics. In fact, we have used the first kinematic model as a basis for an initial kinetic model (D. M. Neustadter, P. E. Crago, and H. J. Chiel, unpublished data).

The limitations of the kinematic models that we have described suggest several possible modifications to improve their accuracy. First, it would be very useful to obtain more data on the actual changes in the shapes of the I3 muscle bands *in vivo*, to improve further the accuracy of the representation of the anterior compartment of the buccal mass. Second, instead of using fixed volumetric databases that are valid over only a part of the range of movement of the radula/odontophore, we could create a kinematic model of the radula/odontophore using the constraints (1) that the radular surface area does not change, since it is topographically a single sheet of inelastic tissue, (2) that the odontophore must maintain a fixed volume as any of its linear dimensions changes, and (3) that the I4 muscle will tend to contract preferentially in the direction determined by its embedded bolsters. Third, it might be possible to capture more details of the deformations that occur within the buccal mass by making use of finite element techniques or continuum mechanical models (Fung, 1993).

A clear lesson that we have learned in the process of constructing these different models is the value of starting with the simplest, most analytically tractable model and then adding the least complexity that explains as many of the data as possible. If this is carried out in close conjunction with experimental work, modeling and experiments mutually influence and focus one another. This is preferable to waiting until most of the data are in hand before even beginning to construct a model. In spite of the limitations that we have discussed, the quantitative agreement between the predictions of the second kinematic model and the experimental data gives us some confidence in the predictions that we make below.

Comparison of in vivo *and* in vitro *data with the second kinematic model*

There are some discrepancies between the kinematics observed *in vivo*, *in vitro* and in the second model. The observed *in vivo* changes in the antero-posterior length of the buccal mass are similar in amplitude but somewhat different

in phasing from those observed *in vitro* and predicted by the model. In all three cases, the length is a minimum in protraction. However, the model predicts (and the *in vitro* data show) that the maximum antero-posterior length is observed at the peak of retraction, whereas the peak length *in vivo* occurs after the peak of retraction, at the time when the full retraction shape is no longer observed and the buccal mass begins to move anteriorly (end of the *t3* interval). It is likely that the reason for this discrepancy is that the fully extended radula/odontophore complex (Fig. 4C; also see Fig. 10A in Drushel *et al.* 1997) bulges out through the thin I2 muscle as it begins to protract, causing the entire length of the buccal mass to increase further than it did when this structure was fully retracted (compare Fig. 4C and D). We did not observe this full retraction shape during the *in vitro* motor programs induced by dopamine. This may be due to the differences between the motor program induced pharmacologically and that induced by physiological stimuli. It is also possible that, in the presence of a large mechanical load, the buccal mass assumes different shapes in order to grasp and tear food more effectively (Hurwitz and Susswein, 1992). This is also likely to explain the smooth, sinusoidal changes in length observed *in vitro*, as opposed to the jerkier movements observed *in vivo* as the radula snaps back after tearing off a piece of food (based on observations of video tapes of intact, transilluminated animals). The discrepancy between the model prediction and the *in vivo* observations is consistent with the inability of the 'retracted' volumetric database to reproduce the *in vivo* shape of the buccal mass in full retraction (Fig. 6H).

Another discrepancy between the *in vivo* and *in vitro* data is that the maximum amplitude of the antero-posterior buccal mass length and its overall net change are nearly constant over several cycles *in vivo* but increase greatly during the *in vitro* motor programs (compare Figs 9 and 10, open circles). This increasing intensity is reminiscent of other arousal phenomena that have been observed in *Aplysia* species in response to another biogenic amine, serotonin (Weiss *et al.* 1981; Rosen *et al.* 1989). In contrast, the *in vivo* movements were performed by an animal that was fully aroused and engaged in feeding behavior, and thus may not show this progressive increase in intensity.

Implications for buccal mass function and neural control

Despite the limitations of the kinematic models discussed above, they do allow us to make testable inferences about the function of components of the buccal mass. These inferences are similar to, but more detailed than, those made by Howells (1942) on the basis of his functional anatomical studies of the buccal mass.

Position of the radular surface

The kinematic models assume that the radular surface moves from between the jaws near the peak of protraction to the opening of the esophagus at the peak of retraction. This is a reasonable assumption, since the feeding system must transport food continuously from the jaws to the esophagus. The data from the stained *Aplysia californica* provide an empirical basis for this assumption and are the first description of the positions of the radular surface when it is not visible between the jaws in intact, behaving animals during feeding. Although it would be interesting to describe the continuous changes in position of the radular surface during feeding, we did not choose to do so for this study. The first kinematic model does generate a continuous prediction of the location of the radular surface but, because of its inaccuracies in predicting overall buccal mass shape, its prediction was not tested quantitatively. The second kinematic model only provides discontinuous information about radular surface location, because it uses discrete volumetric databases.

Changes in antero-posterior buccal mass length

The kinematic models predict that the antero-posterior length of the buccal mass will be at a minimum near the peak of protraction and at a maximum near the peak of retraction. The experimental data suggest that this is likely to be true, but that different feeding programs may be associated with different overall changes in antero-posterior buccal mass length.

During biting, it is likely that the antero-posterior buccal mass length will reach its smallest absolute value near peak protraction as the radula/odontophore complex passes through the jaws (Fig. 5A, frame 108), but that the absolute value near peak retraction will be smaller than that of other feeding responses, since biting is associated with relatively weak retraction movements. During swallowing, if there is relatively little mechanical load, the antero-posterior length should be a minimum at the peak of protraction, but the absolute minimum value is likely to be larger than during biting (during swallowing, the radula will not protract much further than frame 63 in Fig. 5A). The antero-posterior length may be a maximum in full retraction, and the actual maximum value is likely to be greater than during biting, since the radula/odontophore retracts further than it does during biting (see Fig. 5A, frame 0). During swallowing against a large mechanical load, or during tearing, our data suggest that the peak antero-posterior length will occur after the peak of retraction, as the fully extended radula/odontophore (see Fig. 10A in Drushel *et al.* 1997; Fig. 4C) begins to protract and bulges through the thin I2 muscle.

During rejection responses, it is possible that the largest variations in antero-posterior buccal mass length may be observed, since the radula/odontophore complex must both strongly retract (to grasp material to be pulled out of the buccal cavity) and strongly protract (to push the material out of the buccal cavity). In the future, it may be possible to test these hypotheses using studies of transilluminated animals. These studies may also clarify the likely sites of modification of motor neuronal output necessary to generate these different variations of the basic protraction/retraction motor program.

Position of the lateral groove

We studied the positions of the lateral groove using the

models and an *in vitro* preparation. Knowing the position of the lateral groove was essential for defining the border between the I1 and I2 muscles on outlines of the buccal mass. The second kinematic model, which more accurately matched the shapes observed *in vivo*, predicted that the lateral groove was essentially midway between the anterior and posterior extents of the buccal mass throughout the feeding cycle, varying from 45 % to 53 %, and these percentages were similar to those observed *in vitro*, even though the *in vitro* buccal mass manifested much larger excursions in its antero-posterior length during its rhythmic sequences of protractions and retractions. These results suggest that the cartilages of the jaw are not sufficiently rigid so that the entire anterior compartment of the buccal mass maintains a fixed length throughout the protraction/retraction cycle. Rather, the margin of the anterior compartment, the lateral groove, remains at approximately 50 % of the antero-posterior length of the buccal mass throughout the feeding cycle, as it would be expected to do if it were merely a superficial landmark at the midpoint of the surface of the buccal mass. However, both the second kinematic model and the *in vitro* data suggest that the length of the anterior compartment is not a fixed percentage of the antero-posterior length. The variations in the percentages observed indicate that the anterior compartment can lengthen or shorten independently of the entire buccal mass. In turn, this suggests that, during the feeding cycle, the neural control of the buccal mass may act to reduce or increase the size of the anterior compartment independently of the size of the posterior compartment. This may be useful if compressing the anterior compartment prevents the radula/odontophore from being pulled anteriorly in response to a large mechanical load and may help the jaws clamp down on a piece of seaweed that will then be torn by a rapid posterior movement of the radula/odontophore.

Role of the I3 muscle

A consequence of the assumption that the I3 muscle bands are isovolumetric in both kinematic models is that, during the retraction phase of feeding, the annular diameter of each of the muscle bands decreases and the cross-sectional radius increases, whereas during the protraction movements of biting, the annular diameter increases and the cross-sectional radius decreases. Since the cross-sectional diameter of each of the tori in the first kinematic model is uniform, the decrease in cross-sectional diameter is clearly evident in the lateral views of the model (Fig. 5A). In contrast, in the second kinematic model, the maximum cross-sectional diameter occurs midway along the dorso-ventral length of a ring (see Fig. 2D, rings 1–6). Thus, the maximum cross-sectional diameters of the rings are not visible in lateral view (Fig. 6A–G), but the second kinematic model does predict that I3 muscle bands have their minimum overall cross-sectional radius when the radula/odontophore complex protracts through them. It also predicts that the maximum change in length of the I3 muscle bands will occur midway along the dorso-ventral length of the buccal mass and that the minimum change will occur at its dorsal and ventral insertions into the jaw cartilages.

Both kinematic models suggest that different bands of the I3 muscle play different functional roles depending on the relative position of the radula/odontophore (e.g. Fig. 5A, frames 108 and 89): bands that are posterior to the mid-point of the radula/odontophore will tend to protract it as they constrict, whereas bands that are anterior to the mid-point of the radula/odontophore will tend to retract it as they constrict. The models also strongly suggest that the mechanical advantage of any of the I3 muscle bands depends critically upon its position relative to the midpoint of the radula/odontophore complex. A band that is slightly posterior to the mid-point will have far less mechanical advantage than one that is almost fully posterior to the whole radula/odontophore complex. However, more intense activation of the fully posterior band will be needed to cause it to constrict sufficiently for it to contact the radula/odontophore. Similar effects should be observed in bands just anterior to the mid-point as opposed to those fully anterior. These observations suggest that the timing and coordination of the activation of the I3 muscle bands is very important for generating appropriate protraction and retraction movements. It is intriguing that experimental studies of the I3 muscle bands have demonstrated that its anterior, medial and posterior regions are differentially activated and receive differential motor innervation (Nagahama and Takata, 1988, 1989; Cohen and Kirk, 1990).

Role of the I2 muscle

Both kinematic models suggest that protraction is associated with a shortening of the I2 muscle and retraction with a lengthening of the I2 muscle. In fact, the I2 muscle receives motor neuronal input during the protraction phase of feeding responses, and lesions of the I2 muscle or of its innervation severely disrupt the translational component of protraction (Hurwitz *et al.* 1996). Lesions of I2 do not eliminate the rotational component of protraction, which is presumably due to the rotation of the radula/odontophore about the ‘hinge’ formed by the interdigitating I4 and I3 musculature. Recordings from the I2 muscle demonstrate that it also receives significant activation during the retraction phase of feeding when the radula/odontophore complex is subjected to significant mechanical loading (Hurwitz *et al.* 1996), suggesting that it may also play some role in the braking movements of the radula/odontophore during retraction or assist in compressing the radula/odontophore.

The modeling, *in vivo* and *in vitro* data presented in this paper can be combined to predict the relationship between the neural activation of the I2 muscle and its kinematics (Fig. 12). Activity in B31/B32 and B61/B62, which is responsible for the initial fast EMG activity recorded in the I2 muscle (Hurwitz *et al.* 1996), begins in the *t4* interval (start of anterior buccal mass movement to peak of protraction) and ends early in *t1* (after the peak of protraction). The muscle then lengthens as a consequence of the posterior movement of the radula/odontophore complex, presumably due both to the rotation of the radula/odontophore about the hinge and to

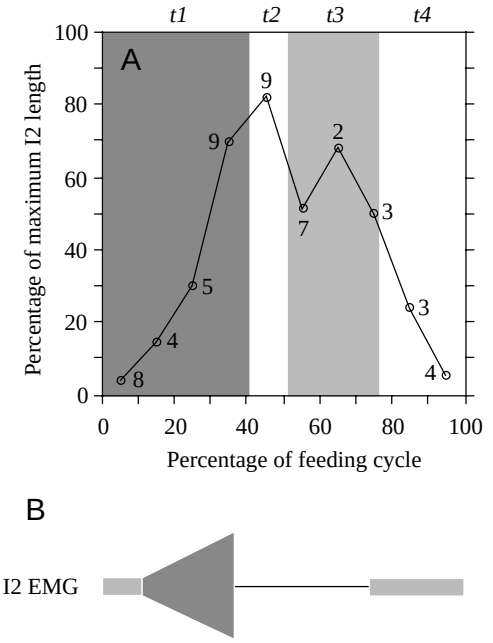

Fig. 12. Schematic correlation of I2 kinematics (A) with the timing of I2 electromyographic (EMG) activity (B). Raw kinematic data from which the averaged kinematic data are calculated are shown in Fig. 11. Periods *t1–t4* are defined in Fig. 9. EMG data are derived from Hurwitz *et al.* (1996) and the data shown in Fig. 10B by rescaling the individual timebases to a single feeding cycle length. Data are scaled to the length of the cycle (0 % is the start of the cycle, 100 % is the end of the cycle) and maximum length change (0 % is the minimum length, 100 % is the maximum length). Small, fast EMG inputs due to B31/ B32 and B61/ B62 are indicated by a light gray rectangle. Slower, facilitating EMG inputs are indicated by a darker gray trapezoid. Note that the onset of the small, fast EMG precedes the peak contraction of the I2 muscle, which reaches its minimum length in protraction (start of *t1*). The number of feeding responses (out of nine) in which it was possible to estimate the I2 length at this time in the cycle is indicated for each data point.

constriction of the I1/I3 muscles, which forces the radula/odontophore posteriorly. During this time, a slower, facilitating burst of EMG activity is observed, whose magnitude is related to the mechanical load on the buccal mass. If this input activates the I2 muscle, it could help I2 to brake abrupt retraction movements of the sort observed during tearing or to compress the radula/odontophore during retraction. This is consistent with our observations that, in response to rapid stretch when it is activated, I2 generates strong braking forces (Fig. 7A in Yu *et al.* 1997).

The muscle reaches its peak length in retraction. Unpublished observations (S.-N. Yu, P. E. Crago and H. J. Chiel) indicate that this length is close to the optimal length for force generation in I2. In two of the nine swallows *in vivo*, I2 also lengthened during the *t3* interval (Fig. 12). This secondary lengthening may be due to the extended radula/odontophore shape bulging posteriorly into the thin I2 muscle as the radula/odontophore begins to rotate anteriorly. It is interesting to note that I2 begins to shorten (middle of *t3*) before neural activation occurs (at the *t3*/*t4* border). This suggests that the passive properties of I2 may act in a complementary fashion to its neural control, contributing to the onset of muscle shortening at the beginning of the protraction phase.

Supported by NIH grant HL-25830 and Whitehall Foundation grant M97-12. We thank Drs Randall D. Beer and Joseph Mansour for their helpful suggestions in formulating the first kinematic model and two anonymous referees for their comments on an earlier draft of the manuscript.

References

CHAPMAN, G. (1958). The hydrostatic skeleton in the invertebrates. *Biol. Rev.* **33**, 338–371.

CHAPMAN, G. (1975). Versatility of hydraulic systems. *J. exp. Zool.* **194**, 249–270.

CHIEL, H. J., CRAGO, P., MANSOUR, J. M. AND HATHI, K. (1992). Biomechanics of a muscular hydrostat: A model of lapping by a reptilian tongue. *Biol. Cybernetics* **67**, 403–415.

CHIEL, H. J. AND SUSSWEIN, A. J. (1993). Learning that food is inedible in freely-behaving *Aplysia californica*. *Behav. Neurosci.* **107**, 327–338.

CHURCH, P. J. AND LLOYD, P. E. (1994). Activity of multiple identified motor neurons recorded intracellularly during evoked feedinglike motor programs in *Aplysia*. *J. Neurophysiol.* **72**, 1794–1809.

COHEN, K. P. AND KIRK, M. D. (1990). Individual buccal motoneurons of *Aplysia californica* innervate multiple buccal muscles and display unique neuromuscular synaptic plasticities. *Soc. Neurosci. Abstr.* **16**, 1227.

DEMONT, M. E. (1992). Locomotion of soft bodied animals. In *Mechanics of Animal Locomotion*, vol. 11 (ed. R. McN. Alexander), pp. 167–190. Berlin: Springer-Verlag.

DRUSHEL, R. F., CHIEL, H. J. AND CRAGO, P. E. (1994). Static- and dynamic- radula/odontophore kinematic models of the buccal mass of *Aplysia californica*. *Soc. Neurosci. Abstr.* **20** (Part 2), 1597.

DRUSHEL, R. F., CRAGO, P. E. AND CHIEL, H. J. (1993). The muscular hydrostatic structure of the buccal mass of *Aplysia californica*. *Soc. Neurosci. Abstr.* **19** (Part 2), 1599.

DRUSHEL, R. F., NEUSTADTER, D. M., SHALLENBERGER, L. L., CRAGO, P. E. AND CHIEL, H. J. (1997). The kinematics of swallowing in the buccal mass of *Aplysia californica*. *J. exp. Biol.* **200**, 735–752.

EALES, N. B. (1921). *Aplysia*. *LMBC Memoir XXIV*. Liverpool: Liverpool University Press. 91pp.

ELLIOTT, C. J. H. AND BENJAMIN, P. R. (1985*a*). Interactions of pattern-generating interneurons controlling feeding in *Lymnaea stagnalis*. *J. Neurophysiol.* **54**, 1396–1411.

ELLIOTT, C. J. H. AND BENJAMIN, P. R. (1985*b*). Interactions of the slow oscillator interneuron with feeding pattern-generating interneurons in *Lymnaea stagnalis*. *J. Neurophysiol.* **54**, 1412–1421.

FUNG, Y. C. (1993). *Biomechanics: Mechanical Properties of Living Tissues*. New York: Springer-Verlag. 568pp.

GETTING, P. A. AND DEKIN, M. S. (1985). *Tritonia* swimming: A model system for integration within rhythmic motor systems. In *Model Neural Networks and Behavior* (ed. A. I. Selverston), pp. 3–20. New York: Plenum Press.

HOWELLS, H. H. (1942). The structure and function of the alimentary canal of *Aplysia punctata*. *Q. Jl. microsc. Sci.* **83**, 357–397.

HURWITZ, I., KUPFERMANN, I. AND SUSSWEIN, A. J. (1997). Different roles of neurons B63 and B34 that are active during the protraction phase of buccal motor programs in *Aplysia californica*. *J. Neurophysiol.* **78**, 1305–1319.

HURWITZ, I., NEUSTADTER, D., MORTON, D. W., CHIEL, H. J. AND SUSSWEIN, A. J. (1996). Activity patterns of the B31/B32 pattern initiators innervating the I2 muscle of the buccal mass during normal feeding movements in *Aplysia californica*. *J. Neurophysiol.* **75**, 1309–1326.

HURWITZ, I. AND SUSSWEIN, A. (1992). Adaptation of feeding sequences in *Aplysia oculifera* to changes in the load and width of food. *J. exp. Biol.* **166**, 215–235.

HURWITZ, I. AND SUSSWEIN, A. J. (1996). B64, a newly-identified central pattern generator element producing a phase switch from protraction to retraction in buccal motor programs of *Aplysia californica*. *J. Neurophysiol.* **75**, 1327–1344.

JORDAN, R., COHEN, K. P. AND KIRK, M. D. (1993). Control of intrinsic buccal muscles by motoneurons B11, B15 and B16 in *Aplysia californica*. *J. exp. Zool.* **265**, 496–506.

KANDEL, E. R. (1976). *Cellular Basis of Behavior*. San Francisco: W. H. Freeman. 727pp.

KATER, S. B. (1974). Feeding in *Helisoma trivolvis*: The morphological and physiological bases of a fixed action pattern. *Am. Zool.* **14**, 1017–1036.

KATZ, P. S. AND FROST, W. N. (1996). Intrinsic neuromodulation: altering neuronal circuits from within. *Trends Neurosci.* **19**, 54–61.

KIER, W. M. AND SMITH, K. K. (1985). Tongues, tentacles and trunks: The biomechanics of movement in muscular-hydrostats. *Zool. J. Linn. Soc.* **83**, 307–324.

KRISTAN, W. B., JR, SKALAK, R., WILSON, R. J. A., SKIERCZYNSKI, B. A., MURRAY, J. A., EISENHART, F. J. AND CACCIATORE, T. W. (1998). Biomechanics of hydroskeletons: Lessons learned from studies of crawling in the medicinal leech. In *Biomechanics and Neural Control of Movement* (ed. J. M. Winters and P. E. Crago). New York: Springer-Verlag (in press).

KUPFERMANN, I. AND WEISS, K. R. (1982). Activity of an identified serotonergic neuron in free moving *Aplysia* correlates with behavioral arousal. *Brain Res.* **241**, 334–337.

LOCKERY, S. R. AND KRISTAN, W. B., JR (1990*a*). Distributed processing of sensory information in the leech. I. Input–output relations of the local bending reflex. *J. Neurosci.* **10**, 1811–1815.

LOCKERY, S. R. AND KRISTAN, W. B., JR (1990*b*). Distributed processing of sensory information in the leech. II. Identification of interneurons contributing to the local bending reflex. *J. Neurosci.* **10**, 1816–1829.

MORTON, D. W. AND CHIEL, H. J. (1993). The timing of activity in motor neurons that produce radula movements distinguishes ingestion from rejection in *Aplysia*. *J. comp. Physiol.* A **173**, 519–536.

NAGAHAMA, T. AND TAKATA, M. (1988). Food-induced firing patterns in motoneurons producing jaw movements in *Aplysia kurodai*. *J. comp. Physiol.* A **162**, 729–738.

NAGAHAMA, T. AND TAKATA, M. (1989). Neural mechanisms generating firing patterns in jaw motoneurons during the food-induced response in *Aplysia kurodai*. *J. comp. Physiol.* A **166**, 143–150.

NEUSTADTER, D., CHIEL, H. J., CRAGO, P. E., MANSOUR, J. AND BEER, R. D. (1992). A model of the buccal mass of *Aplysia*. *Third International Conference of Neuroethology. Montreal, Canada*. Abstract 190.

OZKAYA, N. AND NORDIN, M. (1991). *Fundamentals of Biomechanics: Equilibrium, Motion and Deformation*. New York: Van Nostrand Reinhold. 396pp.

PLUMMER, M. R. AND KIRK, M. D. (1990). Premotor neurons B51 and B52 in the buccal ganglia of *Aplysia californica*: Synaptic connections, effects on ongoing motor rhythms and peptide modulation. *J. Neurophysiol.* **63**, 539–558.

ROSEN, S. C., WEISS, K. R., GOLDSTEIN, R. S. AND KUPFERMANN, I. (1989). The role of a modulatory neuron in feeding and satiation in *Aplysia*: Effects of lesioning of the serotonergic metacerebral cells. *J. Neurosci.* **9**, 1562–1578.

SCOTT, M. L., GOVIND, C. K. AND KIRK, M. D. (1991). Neuromuscular organization of the buccal system in *Aplysia californica*. *J. comp. Neurol.* **312**, 207–222.

SKIERCZYNSKI, B. A., WILSON, R. J. A., KRISTAN, W. B., JR AND SKALAK, R. (1996). A model of the hydrostatic skeleton of the leech. *J. theor. Biol.* **181**, 329–342.

STARMÜHLNER, F. (1956). Beiträge zur Mikroanatomie und Histologie des Darmkanals einiger Opisthobranchier. I. *Sitzungsberichte d. mathem-naturw. Kl., Abt. I* **165**, 8–152.

SUSSWEIN, A. J., SCHWARZ, M. AND FELDMAN, E. (1986). Learned changes of feeding behavior in *Aplysia* in response to edible and inedible foods. *J. Neurosci.* **6**, 1513–1527.

TEYKE, T., ROSEN, S. C. AND WEISS, K. R. (1993). Dopaminergic neuron B20 generates rhythmic neuronal activity in the feeding motor circuitry of *Aplysia*. *Brain Res.* **630**, 226–237.

TEYKE, T., WEISS, K. R. AND KUPFERMANN, I. (1990). An identified neuron (CPR) evokes neuronal responses reflecting food arousal in *Aplysia*. *Science* **247**, 85–87.

VAN LEEUWEN, J. L. (1997). Why the chameleon has spiral-shaped muscle fibres in its tongue. *Phil. Trans. R. Soc. Lond. B* **352**, 573–589.

VAN LEEUWEN, J. L. AND KIER, W. M. (1997). Functional design of tentacles in squid: Linking sarcomere ultrastructure to gross morphological dynamics. *Phil. Trans. R. Soc. Lond. B* **352**, 551–571.

WATSON, J. E. AND RITZMANN, R. E. (1997*a*). Leg kinematics and muscle activity during treadmill running in the cockroach, *Blaberus discoidalis*. I. Slow running. *J. comp. Physiol.* A **182**, 11–22.

WATSON, J. T. AND RITZMANN, R. E. (1997*b*). Leg kinematics and muscle activity during treadmill running in the cockroach, *Blaberus discoidalis*. II. Fast running. *J. comp. Physiol.* A **182**, 23–33.

WEISS, K. R., BREZINA, V., CROPPER, E. C., HOOPER, S. L., MILLER, M. W., PROBST, W. C., VILIM, F. S. AND KUPFERMANN, I. (1992). Peptidergic co-transmission in *Aplysia*: Functional implications for rhythmic behaviors. *Experientia* **48**, 456–463.

WEISS, K. R., COHEN, J. L. AND KUPFERMANN, I. (1978). Modulatory control of buccal musculature by a serotonergic neuron (metacerebral cell) in *Aplysia*. *J. Neurophysiol.* **41**, 181–203.

WEISS, K. R., KOCH, U. T., KOESTER, J., MANDELBAUM, D. E. AND KUPFERMANN, I. (1981). Neural and molecular mechanisms of food-induced arousal in *Aplysia californica*. In *Neurobiology of Invertebrates*, vol. 23 (ed. J. Salanki), pp. 305–344. Budapest: Akademiai Kiado.

WILSON, R. J. A., SKIERCZYNSKI, B. A., BLACKWOOD, S., SKALAK, R. AND KRISTAN, W. B., JR (1996*a*). Mapping motor neurone activity to overt behaviour in the leech: internal pressures produced during locomotion. *J. exp. Biol.* **199**, 1415–1428.

WILSON, R. J. A., SKIERCZYNSKI, B. A., MEYER, J. K., SKALAK, R. AND KRISTAN, W. B., JR (1996*b*). Mapping motor neuron activity to overt behavior in the leech. I. Passive biomechanical properties of the body wall. *J. comp. Physiol.* **178**, 637–654.

WITTENBERG, G. AND KRISTAN, W. B., JR (1992*a*). Analysis and

modeling of the multisegmental coordination of shortening behavior in the medicinal leech. I. Motor output pattern. *J. Neurophysiol.* **68**, 1683–1692.

WITTENBERG, G. AND KRISTAN, W. B., JR (1992*b*). Analysis and modeling of the multisegmental coordination of shortening behavior in the medicinal leech. II. Role of identified interneurons. *J. Neurophysiol.* **68**, 1693–1707.

YAMAGUCHI, G. T. AND ZAJAC, F. E. (1990). Restoring unassisted natural gait to paraplegics *via* functional neuromuscular stimulation: a computer simulation study. *IEEE Trans. biomed. Eng.* **37**, 886–902.

YU, S.-N., CRAGO, P. E. AND CHIEL, H. J. (1997). A nonisometric kinetic model for smooth muscle. *Am. J. Physiol.* **272**, C1025–C1039.

ZAJAC, F. E. (1993). Muscle coordination of movement: A perspective. *J. Biomechanics* **26** (Suppl. 1), 109–124.